

POLITECNICO DI TORINO

Master's Degree in Biomedical Engineering



**Analysis of the effect of the respiration on features
extracted from the electrocardiogram
and the heart sounds**

Supervisors

Prof. Ing. Marco Knaflitz
Ing. Noemi Giordano

Candidate

Alice Lolli

Academic Year 2024/2025

Summary

Respiration is known to influence cardiac signals through the modulation of both cardiac activity and thoracic motion. The respiratory contribution on the modulation of the electrocardiogram (ECG) both in amplitude and frequency is well established. On the other side, similar respiratory-related variations may also affect heart sounds, visible in the phonocardiogram (PCG). In this study, both ECG and PCG signals were analyzed to evaluate the influence of respiration on these signals and, in particular, its impact on the timing of heart valve closures. The latter have a clinical application in noninvasively assessing the hemodynamics of the heart. In this context, the aim of this thesis is to assess whether accounting for respiratory information could improve the accuracy of Cardiac Time Intervals (CTIs) estimation. To this end, a multi-sensor device comprising ECG, PCG, and a triaxial accelerometer was used for respiratory detection. The respiratory signal was extracted from the accelerometer data, and points of maximum and minimum thoracic expansion were identified to assess the influence of respiration on CTIs estimation. The ECG was used as a temporal reference for heart sounds latency estimation, whereas the PCG was employed to estimate the respiratory impact on the timing of valve closure events. Moreover, the respiratory signal was extracted from the measured accelerations. Then, the estimates of the CTIs in different respiratory phases were compared. In the analyzed group of subjects, no relevant differences in the estimated valvular time of closure were observed, although statistically significant conclusions could not be drawn due to the limited number of subjects. From field application perspective, these findings suggest that explicit knowledge of the respiratory signal is probably not necessary for accurate estimation of CTIs. To obtain a statistically sound answer to the main question, a more extensive study is needed, that is beyond the scope of this thesis. Results herein reported should be considered as a pilot study that produced some of the data necessary to estimate the minimum size of the sample population to be considered for a statistically sound study.

Contents

| | |
|--|-----|
| List of Abbreviations | V |
| List of Figures | VII |
| List of Tables | IX |
| 1 Introduction | 1 |
| 1.1 Clinical motivation: Acute Heart Failure Prevention and Home Monitoring . | 1 |
| 1.1.1 Overview of Heart Failure | 1 |
| 1.1.2 Management of Heart Failure | 3 |
| 1.1.3 Clinical needs and motivation for Home Monitoring | 4 |
| 1.2 Cardiac Time Intervals as Non-Invasive Markers of Cardiac Function | 5 |
| 1.3 Respiratory Influence on Cardiovascular Signals | 6 |
| 1.4 Research Hypothesis and Objectives | 7 |
| 1.5 Structure of the Thesis | 7 |
| 2 State of the Art | 9 |
| 2.1 ECG and PCG in Cardiac Monitoring | 9 |
| 2.2 Detection of Heart Sounds and Estimation of CTIs | 9 |
| 2.3 Wearable ECG-PCG Devices for Cardiac Monitoring | 10 |
| 2.4 Approaches to Respiratory Signal Estimation | 10 |
| 2.4.1 Respiration Estimation from Accelerometric Signals | 11 |
| 2.4.2 Respiration Estimation from Biosignals | 11 |
| 2.5 Effect of Respiratory Phase on CTIs Accuracy | 12 |
| 2.6 Open Challenges in the Interaction Between Respiratory and Cardiovascular Signals | 13 |
| 3 Materials and Methods | 15 |
| 3.1 Description of the Wearable Device | 15 |
| 3.2 Data Acquisition Protocol | 16 |
| 3.3 Methods for Estimating the Respiratory Signal | 16 |
| 3.3.1 Accelerometer-derived respiration | 17 |
| 3.3.2 ECG-derived respiration | 17 |
| 3.3.3 PCG-derived respiration | 20 |
| 3.3.4 Cardiac latency-derived respiration | 22 |
| 3.3.5 Interpolation of discrete respiratory estimates | 23 |
| 3.3.6 Common Processing Pipeline | 24 |
| 3.4 Identification of Respiratory Phases and Characteristic Points | 25 |
| 3.5 Estimation of Cardiac Latencies | 27 |
| 3.5.1 Global estimation of cardiac latencies | 27 |
| 3.5.2 Respiration-conditioned estimation of cardiac latencies | 28 |

| | | |
|----------|--|-----------|
| 3.5.3 | Method A: Phase-based classification of cardiac cycles | 28 |
| 3.5.4 | Method B: Latency estimation around respiratory maxima and minima | 29 |
| 3.5.5 | Method C: Latency estimation before and after respiratory transitions | 30 |
| 3.5.6 | Estimation of Cardiac Time Intervals | 31 |
| 3.6 | Interpretation of CTIs Variations | 32 |
| 4 | Results | 33 |
| 4.1 | Respiratory Rate Estimation Across Methods | 33 |
| 4.2 | Inter-subject Distribution of CTIs | 35 |
| 4.3 | Global Latency Validation | 40 |
| 4.4 | Phase-Specific Latency Validation | 40 |
| 4.5 | Subject-Specific Percentage Variations Between Global and Phase-Specific CTIs | 41 |
| 5 | Discussion | 47 |
| 5.1 | Reliability of Respiratory Signal Extraction Methods | 47 |
| 5.2 | Validation of Cardiac Estimates | 48 |
| 5.2.1 | Global Validation | 48 |
| 5.2.2 | Phase-Specific Validation | 48 |
| 5.3 | Verification of the Research Hypothesis | 48 |
| 5.3.1 | Group-Level Distribution Analysis | 48 |
| 5.4 | Subject-Specific Interpretation of Respiratory Modulation on CTIs | 49 |
| 6 | Conclusion | 51 |
| 6.1 | Limitations of the Current Study | 51 |
| 6.1.1 | Final Remarks and Future Research Directions | 51 |
| | Bibliography | 53 |

List of Abbreviations

| | |
|----------------|---|
| AHF | Acute Heart Failure |
| AM | Amplitude Modulation |
| BNP | B-type Natriuretic Peptides |
| bpm | Breaths per minute |
| BW | Baseline Wander |
| CHF | Chronic Heart Failure |
| CI | Confidence Interval |
| CMR | Cardiac Magnetic Resonance |
| CTCA | Computed Tomography Coronary Angiography |
| CTI | Cardiac Time Interval |
| CVD | Cardiovascular Disease |
| DC | Direct Current |
| ECG | Electrocardiogram |
| EDR | ECG-Derived Respiration |
| EE | Energy Expenditure |
| EMAT | Electromechanical Activation Time |
| FM | Frequency Modulation |
| HF | Heart Failure |
| HFimpEF | Heart Failure with improved Ejection Fraction |
| HFpEF | Heart Failure with preserved Ejection Fraction |
| HFrEF | Heart Failure reduced Ejection Fraction |
| HFmrEF | Heart Failure with mildly reduced Ejection Fraction |
| HR | Heart Rate |
| ICA | Independent Component Analysis |
| LVEF | Left Ventricular Ejection Fraction |

LVET Left Ventricular Ejection Time
LVST Left Ventricular Systolic Time
MIMU Miniaturized Magneto-Inertial Measurement Unit
MSE Mean Square Error
NT-proBNP N-terminal fragment of pro-BNP
PCA Principal Component Analysis
PCG Phonocardiogram
PCHIP Piecewise Cubic Hermite Interpolation
PDR PCG-Derived Respiration
PEP Pre-Ejection Period
PZT Lead Zirconate Titanate
QRS QRS Complex
RSA Respiratory Sinus Arrhythmia
RVST Right Ventricular Systolic Time
SCG Seismocardiogram
SE Shannon Energy
SNR Signal-to-Noise Ratio
SPECT Single-Photon Emission Computed Tomography
STFT Short-Time Fourier Transform
S₁ First heart sound
S₂ Second heart sound
TST Total Systolic Time
VHP Peak-to-peak heart-period variation

List of Figures

| | | |
|------|--|----|
| 1.1 | Diagnostic algorithm for HF | 4 |
| 3.1 | Recording system. Array to record ECG, PCG and accelerometric signals . . | 15 |
| 3.2 | Preprocessing of the triaxial accelerometer signal. The raw acceleration along the three axes was corrected for DC offset, combined into a single waveform through the Euclidean norm, and downsampled to obtain the resulting acceleration norm. | 17 |
| 3.3 | Comparison between the reference (A) and modified (B) algorithms for R-peak detection, with the modification enforcing a 0.35 s refractory period and an amplitude-slope criterion to retain the most representative peak, thereby preventing false multiple. | 18 |
| 3.4 | Detection of R-R intervals in the ECG signal. Consecutive R peaks (red markers) were identified using the modified Pan-Tompkins algorithm, and the R-R interval was computed as the temporal distance between successive peaks. | 19 |
| 3.5 | Detection of R and S peaks in the ECG signal. The positions of R peaks (red markers) and S peaks (green markers) were identified for the computation of the respiratory signal through amplitude modulation (AM). | 19 |
| 3.6 | Shannon envelope of the PCG signal from the selected channel and identification of S_1 peaks. | 21 |
| 3.7 | Shannon envelope of the PCG signal from the selected channel and identification of S_2 peaks. | 22 |
| 3.8 | Detection of the S_{1m} and S_{1t} components of S_1 on the Shannon envelope of the PCG signal, synchronized with the ECG trace and the corresponding R peaks. | 23 |
| 3.9 | Detection of the S_{2a} and S_{2p} components of S_2 on the Shannon envelope of the PCG signal, aligned with the ECG trace and the corresponding R peaks. | 23 |
| 3.10 | Processing pipeline applied to the norm of the acceleration signal, used as the respiratory reference. | 25 |
| 3.11 | Detection logic in the ZC-AT algorithm. The left panel shows the confirmation of an expiratory peak (minimum) while in the WRC state; the right panel shows the confirmation of an inspiratory peak (maximum) in the WFC state. In both cases, ICS and DCS criteria are used to validate the zero-crossing as a true respiratory extremum. | 27 |
| 3.12 | R-peak classification based on respiratory phase. Each R-peak was assigned to inspiration or expiration according to its location within respiratory windows delimited by adjacent minima and maxima of the respiratory signal. . . | 29 |

| | | |
|------|---|----|
| 3.13 | Selection of R-peaks near respiratory extrema. For each minimum and maximum of the respiratory signal, the nearest R-peak was identified and retained if its relative distance fell below the threshold computed individually for each subject. Accepted beats are shown as empty circles and color-coded according to their phase, while rejected beats are indicated with red crosses. | 30 |
| 3.14 | R-peaks before and after respiratory extrema. For each maximum or minimum of the respiratory signal, the corresponding R-peaks immediately preceding and following the extremum are shown, together with their assignment to inspiratory or expiratory transitions. | 31 |
| 4.1 | Scatter plot of the estimated respiratory rate across subjects for Methods 1 to 5. | 34 |
| 4.2 | Scatter plot of the estimated respiratory rate across subjects for Methods 1 and 6 to 9. | 35 |
| 4.3 | Distribution of subject-level mean values of EMAT across respiratory conditions defined according to the selection criteria described in Section 3.5. Each box represents the inter-subject variability for a given condition. The values indicated above the boxes (N) represent the total number of detected cardiac events accumulated across all subjects for each condition. | 36 |
| 4.4 | Distribution of subject-level mean values of LVST across respiratory conditions defined according to the selection criteria described in Section 3.5. Each box represents the inter-subject variability for a given condition. The values indicated above the boxes (N) represent the total number of detected cardiac events accumulated across all subjects for each condition. | 37 |
| 4.5 | Distribution of subject-level mean values of RVST across respiratory conditions defined according to the selection criteria described in Section 3.5. Each box represents the inter-subject variability for a given condition. The values indicated above the boxes (N) represent the total number of detected cardiac events accumulated across all subjects for each condition. | 38 |
| 4.6 | Distribution of subject-level mean values of S_1 -split across respiratory conditions defined according to the selection criteria described in Section 3.5. Each box represents the inter-subject variability for a given condition. The values indicated above the boxes (N) represent the total number of detected cardiac events accumulated across all subjects for each condition. | 39 |
| 4.7 | Distribution of subject-level mean values of S_2 -split across respiratory conditions defined according to the selection criteria described in Section 3.5. Each box represents the inter-subject variability for a given condition. The values indicated above the boxes (N) represent the total number of detected cardiac events accumulated across all subjects for each condition. | 40 |

List of Tables

| | | |
|------|---|----|
| 1.1 | Main CTIs | 5 |
| 3.1 | Anthropometric characteristics of the participants. | 16 |
| 3.2 | Explored ranges and final values of the parameters used for respiratory signal segmentation. | 27 |
| 3.3 | Latency values from ECG and PCG components | 31 |
| 4.1 | Estimated respiratory rate (bpm) for each subject – Methods 1 to 5. | 33 |
| 4.2 | Estimated respiratory rate (bpm) for each subject – Methods 1 and 6 to 9. | 34 |
| 4.3 | Global latency comparison | 40 |
| 4.4 | Comparison of phase-specific mean latencies (Inspiration vs. Expiration) across extraction methods (A, B, C-before, C-after) with the reference variability ranges. | 41 |
| 4.5 | Signed percentage variations of EMAT for Method A during inspiration and expiration. | 42 |
| 4.6 | Signed percentage variations of EMAT for Method B during inspiration and expiration. | 42 |
| 4.7 | Signed percentage variations of EMAT for Method C (Before/After) during inspiration and expiration. | 42 |
| 4.8 | Signed percentage variations of LVST for Method A during inspiration and expiration. | 43 |
| 4.9 | Signed percentage variations of LVST for Method B during inspiration and expiration. | 43 |
| 4.10 | Signed percentage variations of LVST for Method C (Before/After) during inspiration and expiration. | 43 |
| 4.11 | Signed percentage variations of RVST for Method A during inspiration and expiration. | 44 |
| 4.12 | Signed percentage variations of RVST for Method B during inspiration and expiration. | 44 |
| 4.13 | Signed percentage variations of RVST for Method C (Before/After) during inspiration and expiration. | 44 |
| 4.14 | Signed percentage variations of S1-split for Method A during inspiration and expiration. | 45 |
| 4.15 | Signed percentage variations of S1-split for Method B during inspiration and expiration. | 45 |
| 4.16 | Signed percentage variations of S1-split for Method C (Before/After) during inspiration and expiration. | 45 |
| 4.17 | Signed percentage variations of S2-split for Method A during inspiration and expiration. | 46 |

| | |
|--|----|
| 4.18 Signed percentage variations of S2-split for Method B during inspiration and expiration. | 46 |
| 4.19 Signed percentage variations of S2-split for Method C (Before/After) during inspiration and expiration. | 46 |

Chapter 1

Introduction

1.1 Clinical motivation: Acute Heart Failure Prevention and Home Monitoring

Cardiovascular diseases (CVDs) represent one of the leading causes of mortality worldwide, contributing substantially to the global burden of disease and imposing a significant strain on healthcare systems in terms of both clinical management and economic costs [1]. This is also confirmed by a recent report from the World Health Organization [1], which highlights the continuous rise in the prevalence of cardiovascular diseases, representing a serious threat to public health. These conditions are often referred to as “silent killers” because, in their early stages, they present with mild or barely recognizable symptoms [2]. Among cardiovascular diseases, heart failure (HF) stands out as one of the most severe and complex to manage, as it is associated with high mortality, frequent hospitalizations, and a significant deterioration in quality of life. Despite the considerable scientific and technological advances achieved in recent years, HF-related mortality has shown a steadily increasing trend since 2011. This evidence underscores the need to adopt an approach that goes beyond the development of pharmacological therapies or life-saving devices, integrating long-term prevention strategies. Such an orientation enables not only more effective disease management but also the possibility of counteracting its onset and progression. In this context, it is essential to promote the advancement of digital technologies and wearable systems capable of ensuring continuous and non-invasive remote monitoring of cardiorespiratory dynamics, thereby supporting a more personalized and proactive model of care [3]. Recent estimates from the Global Burden of Disease Study indicate that the number of individuals living with cardiovascular diseases has nearly doubled over the last three decades, reaching more than 523 million prevalent cases worldwide in 2019 [1]. This dramatic and sustained increase underscores the need for monitoring solutions that extend beyond traditional clinical settings, making continuous home-based assessment a crucial component of effective long-term prevention and management.

1.1.1 Overview of Heart Failure

It is important to provide a general overview of heart failure (HF), which is recognized as a complex and progressive clinical syndrome characterized by the heart’s inability to deliver an adequate cardiac output in relation to the metabolic demands of the body. HF is a clinical syndrome and not a single pathological diagnosis, characterized by key symptoms such as breathlessness, fatigue, and swelling of the lower limbs. These latter may be accompanied by objective signs, including elevated jugular venous pressure, pulmonary crackles, and

peripheral oedema [4]. HF is a condition that evolves over time and, for this reason, progresses through distinct clinical stages, as defined by the American Heart Association and American College of Cardiology (ACC/AHA) heart failure staging system. This classification identifies four stages, from A to D, outlining the continuum from initial risk conditions to the most advanced forms of the disease [5]. A key clinical objective is the prevention of transition between the early stages, particularly the shift from an “at-risk” condition to “pre-HF.” Advances achieved over recent decades in diagnostic techniques, pharmacological therapies, and device-based interventions have led to a change in the demographic profile of patients with HF, who now include individuals with a higher average age. However, this evolution has made clinical management more complex due to the increased frailty of the affected population and the likely presence of multiple comorbidities. The most recent and internationally shared definition describes HF as a syndrome characterized by the presence of symptoms that develop in the context of structural or functional cardiac abnormalities, accompanied by objective evidence of systemic or cardiopulmonary congestion. It derives from a structural and/or functional abnormality of the heart, which consequently leads to increased intracardiac pressures and/or inadequate cardiac output, occurring both at rest and during physical activity [4]. From a clinical perspective, HF is further classified according to left ventricular ejection fraction (LVEF), distinguishing between heart failure with reduced ejection fraction (HFrEF, $EF < 40\%$), mildly reduced ejection fraction (HFmrEF, $41\text{--}49\%$), preserved ejection fraction (HFpEF, $\geq 50\%$), and improved ejection fraction (HFimpEF). systolic function. This categorization allows for differentiation of pathophysiological mechanisms and facilitates the tailoring of therapeutic strategies. At the basis of cardiac dysfunction, it is essential to identify the etiology to formulate an accurate diagnosis, as the underlying pathology determines the most appropriate therapeutic approach [3]. From an epidemiological perspective, HF represents one of the main cardiovascular syndromes, particularly in developed countries, with a prevalence estimated at around 1–2% of the adult population and an incidence of approximately 3–5 new cases per 1000 people per year. Despite improvements in the prevention and management of cardiovascular diseases, population aging has led to an overall increase in the number of cases. Prevalence indeed rises with age, increasing from approximately 1% in individuals under 55 years of age to over 10% in those aged 70 years or older. HFrEF and HFpEF forms appear to be comparable in terms of frequency, although European outpatient registries have reported a higher prevalence of HFrEF. More than half of affected patients are female, confirming the progressive demographic shift associated with this syndrome. Usually, in the majority of cases, HF is due to myocardial dysfunction, either systolic, diastolic, or both. Nevertheless, the development of the syndrome may also be influenced by valvular, pericardial, or endocardial disease, as well as rhythm and conduction disorders [4]. Various clinical conditions are recognized as risk factors associated with the development of heart failure (HF), including hypertension, type 2 diabetes mellitus, ischemic heart disease, obesity, and chronic kidney disease. In particular, hypertension represents one of the most significant causes, as the chronic increase in afterload induces progressive ventricular remodeling and impairment of diastolic function, thereby promoting the evolution toward heart failure [3]. Acute heart failure (AHF) may present as the first clinical episode of the syndrome or, more commonly, as an exacerbation of a previously known chronic condition. Patients with an acute onset tend to have higher in-hospital mortality, but overall show a more favorable post-discharge prognosis, with lower rates of mortality and rehospitalization compared to those with acute decompensation of chronic heart failure (CHF) [6–9]. AHF is defined as the rapid or progressive onset of symptoms and signs related to HF, of such severity as to require urgent medical intervention, often associated with an unplanned hospital admission. It also represents one of the leading causes of hospitalization in individuals over the age of 65. This is one of the reasons why it is associated with high mortality and recurrent

hospital admissions, thereby contributing significantly to the overall healthcare burden of heart failure. The severity of the clinical condition depends on multiple factors, including the interaction between precipitating elements, structural cardiac abnormalities, and concomitant comorbidities, all of which contribute to shaping both in-hospital evolution and long-term prognosis [4].

1.1.2 Management of Heart Failure

In patients with symptoms or risk factors suggestive of HF, the diagnostic workup aims to confirm the presence of cardiac dysfunction and identify the underlying etiology. As recommended by the 2021 European Society of Cardiology (ESC) guidelines [4], the initial evaluation should include ECG and measurement of natriuretic peptides (NPs). A normal ECG and low NP levels—specifically, B-type natriuretic peptides (BNP) <35 pg/mL or N-terminal fragment of pro-BNP (NT-proBNP) <125 pg/mL, make HF unlikely in the non-acute setting. If these initial findings are abnormal, echocardiography represents the key diagnostic tool, providing a comprehensive assessment of cardiac structure and function, including left ventricular ejection fraction (LVEF), wall motion, chamber size, and valve status. Chest X-ray is also recommended to exclude other causes of dyspnoea, such as pulmonary disease, and may support the HF diagnosis by revealing pulmonary congestion or cardiomegaly. These steps are illustrated in the diagnostic algorithm shown in Figure 1.1. In selected patients, additional investigations may help determine the underlying etiology of chronic heart failure. Stress echocardiography can assess inducible ischemia or clarify diagnosis in the presence of valve disease or unexplained dyspnoea. Cardiac magnetic resonance (CMR) imaging provides advanced tissue characterization and identification of myocardial fibrosis or infiltrative diseases. Other modalities, such as computed tomography coronary angiography (CTCA), single-photon emission computed tomography (SPECT), or bone scintigraphy, may be considered in specific clinical contexts to evaluate coronary artery disease or detect cardiac amyloidosis. Accurate diagnosis and optimal chronic treatment are essential to limit disease progression and reduce the risk of AHF, which often arises as a decompensation of a chronic condition and contributes significantly to morbidity and healthcare burden. Pharmacological therapy remains the cornerstone of treatment for HF and should be prioritized before considering device-based strategies. The three primary goals of treatment are: (i) to reduce mortality, (ii) to prevent recurrent hospitalizations due to worsening HF, and (iii) to improve clinical status, functional capacity, and quality of life. Achieving these objectives requires a comprehensive and personalized approach that integrates pharmacotherapy with non-pharmacological measures and continuous monitoring [4].

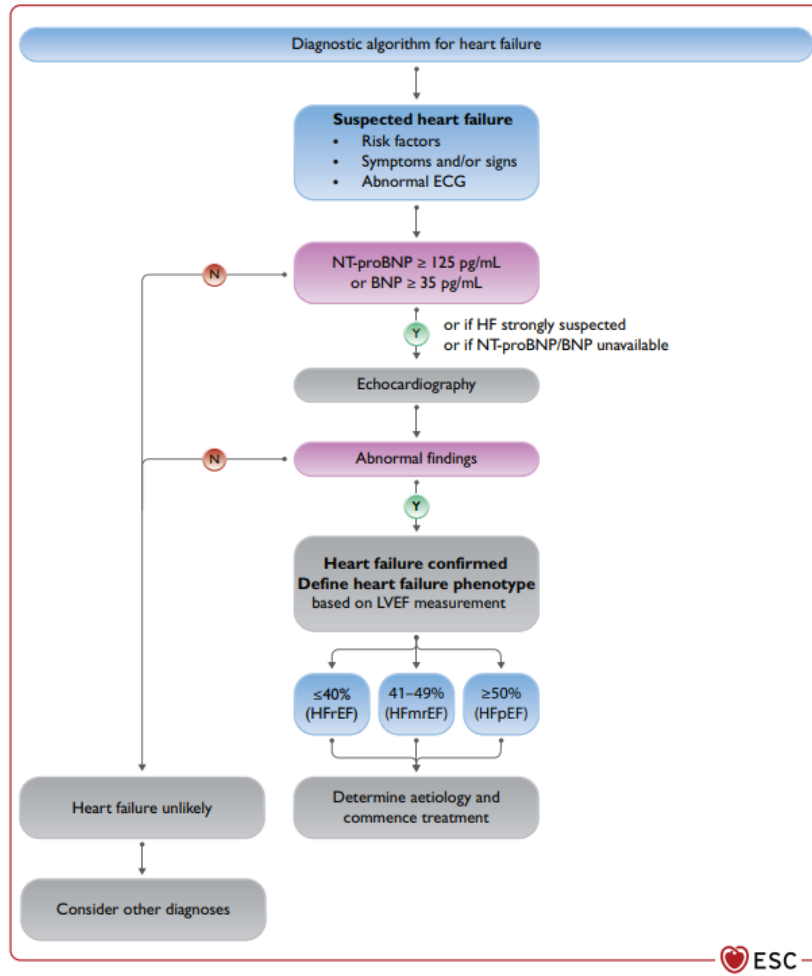


Figure 1.1: Diagnostic algorithm for heart failure as recommended by the ESC guidelines [4].

1.1.3 Clinical needs and motivation for Home Monitoring

Despite advances in diagnosis and clinical management, the follow-up of patients with HF remains complex, particularly after episodes of acute decompensation, when the risk of re-hospitalization is high. One of the main challenges lies in the difficulty of promptly detecting signs of deterioration, which often emerge gradually and in a subclinical manner. Traditional monitoring models, based on periodic check-ups, do not allow for continuous assessment of the patient's physiological status, limiting the possibility of early intervention. In recent years, the evolution of wearable technologies and remote monitoring systems has opened new perspectives both for screening in the general population and for remote surveillance of patients with HF. These devices enable the monitoring of physiological parameters, such as heart rate (HR) and rhythm, respiratory rate, physical activity, posture, blood pressure, weight, sleep, and blood glucose, which may provide useful indications for the early identification of clinical changes potentially associated with decompensation episodes. The LINK-HF trial demonstrated the potential of a multisensor chest patch connected via telemetry to a smartphone, which processes the data through an artificial intelligence algorithm with the aim of predicting exacerbation events several days before actual hospitalization. This approach allows for early detection of clinical deterioration, offering the opportunity to intervene before hospitalization becomes necessary [10]. However, large-scale adoption of such tools remains limited by several factors, including signal noise, inter- and intra-patient

variability, the need for robust algorithms to extract clinically relevant information, and the management of large volumes of data. Beyond technical challenges, operational issues persist, such as device cost, usability, patient engagement and adherence, and the complexity of data processing and interpretation. It is therefore essential to develop monitoring systems that are simple, reliable, and non-invasive, capable of ensuring accurate and stable collection of physiological signals over time and adaptable to a broad user population. Such solutions could significantly contribute to reducing the burden of hospitalizations by improving diagnostic timeliness and continuity of care in the management of HF.

1.2 Cardiac Time Intervals as Non-Invasive Markers of Cardiac Function

Cardiac Time Intervals (CTIs) represent a temporal measure of the sequence of mechanical events occurring during the cardiac cycle and serve as a key indicator of systolic function and electromechanical synchronization of the heart. Among the main intervals considered are the Pre-Ejection Period (PEP), the Left Ventricular Ejection Time (LVET), the Total Systolic Time (TST), and the Electromechanical Activation Time (EMAT). Their estimation enables a non-invasive description of myocardial contractile activity and the temporal coordination between electrical stimulus and mechanical response [11]. Alterations in CTIs have been correlated with various pathological conditions, including mitral valve stenosis, coronary artery disease [12, 13], arterial hypertension [14], atrial fibrillation, hypovolemia, and fluid responsiveness [15], as well as chronic myocardial disease [13]. Importantly, CTIs—especially the PEP and the LVET have demonstrated strong associations with heart failure-related features, such as left ventricular systolic function and ejection fraction [12, 13]. This correlation makes them clinically valuable parameters for evaluating hemodynamic status and for longitudinal monitoring of ventricular function.

Table 1.1: Main CTIs and their physio-clinical significance [11].

| Interval | Definition | Physio-clinical significance |
|-------------|--|--|
| PEP | Time between the onset of ventricular depolarization and the opening of the aortic valve | Reflects myocardial contractility and afterload; its prolongation indicates reduced systolic function or increased peripheral resistance |
| LVET | Interval between the opening and closing of the aortic valve | Represents the duration of ventricular ejection; a reduction is associated with impaired systolic function or elevated afterload |
| TST | Time between the onset of ventricular depolarization and the closure of the aortic valve | Provides an overall measure of mechanical systole duration |
| EMAT | Interval between ventricular electrical activation and the closure of the mitral valve | Indicates the coordination between electrical and mechanical activity; alterations may reflect ventricular asynchrony or contractile dysfunction |

In clinical practice, the opening and closing of cardiac valves are traditionally evaluated using echocardiographic techniques such as M-mode, Doppler, or Tissue Doppler Imaging. However, these methods require skilled operators and are not suitable for continuous

monitoring. For this reason, recent years have seen growing interest in non-invasive and portable techniques for estimating CTIs, based on mechanical and acoustic signals from the chest, such as seismocardiogram (SCG) and phonocardiogram (PCG). Another promising approach involves the combined use of electrocardiogram (ECG) and PCG, which enables direct correlation between the heart’s electrical activity and the mechanical events of valve opening and closure, offering a more comprehensive estimation of cardiac function. These alternative modalities may facilitate early detection of cardiac dysfunction and support timely therapeutic interventions, particularly in outpatient or home settings.

1.3 Respiratory Influence on Cardiovascular Signals

Spontaneous breathing induces cyclic variations in pleural, alveolar, transmural, and intra-abdominal pressures [16], which generate oscillations in venous return, ventricular preload, and afterload. These changes affect the cardiovascular system, producing a phenomenon known as cardiorespiratory coupling [17]. Several physiological mechanisms mediate this interaction: (1) the activation of pulmonary stretch receptors, which are stimulated during inspiration and trigger the Hering–Breuer reflex, inhibiting cardiac vagal motoneurons in the nucleus ambiguus and producing a positive chronotropic effect [17, 18]; (2) the pressure oscillations induced by the thoraco-abdominal pump, which modulate venous return and left ventricular afterload, generating cyclic variations in arterial pressure and activating the baroreflex, associated with a negative chronotropic response during expiration [18–20]; (3) the direct interaction between respiratory circuits in the brainstem and cardiac vagal preganglionic neurons, which contributes to the synchronization between respiratory activity and HR. The overall result of these mechanisms is the respiratory sinus arrhythmia (RSA), which consists of a rhythmic variation of HR synchronized with breathing, characterized by a shortening of the RR interval during inspiration and its prolongation during expiration [21]. RSA represents one of the main forms of cardiorespiratory interaction, together with cardioventilatory coupling, defined by the synchronization between the heartbeat and the onset of inspiration, and respiratory stroke volume synchronization, characterized by the synchronized variation of right and left ventricular stroke volumes over the respiratory cycle [22]. A classic physiological study by Katona and Jih demonstrated that the beat-to-beat variations in RR interval induced by spontaneous breathing, quantified as the peak-to-peak heart-period variation, are strongly and linearly related to parasympathetic heart rate control. The authors reported a high linear correlation between VHP and parasympathetic heart rate control, with an average coefficient of $r = 0.969 \pm 0.024$ (SD), demonstrating that respiratory modulation of the heart period is a strongly vagally mediated phenomenon [23]. Klum et al. [24] proposed a multimodal approach for estimating respiration from ECG and PCG signals, introducing the methods of ECG-derived respiration (EDR) and PCG-derived respiration (PDR). From the ECG signal, respiration is obtained through variations in HR, amplitude, and morphology of the QRS complex (QRS), whereas from the PCG signal it is estimated based on the amplitude, area, and shape oscillations of the first heart sound (S_1) and the second heart sound (S_2), which are themselves modulated by the respiratory cycle. In healthy individuals, this modulation produces small but systematic timing shifts in S_1 , whose physiological split typically ranges between 20 and 30 ms, and more pronounced variations in S_2 , with splitting increasing from approximately 20–30 ms during expiration to about 50 ms in inspiration [25]. In their framework, the PEP is defined as the time between the Q-wave of the ECG and the peak of S_1 in the PCG, while LVET corresponds to the interval between the peaks of S_1 and S_2 . Since the exact timing of valve opening is not directly measurable from surface recordings, the authors use the acoustic signatures of heart sounds as indirect markers of the underlying mechanical

events. In total, twelve beat-to-beat features were extracted, belonging to four main classes: timing (HR, PEP, LVET), area (QRS_{area} , $S1_{\text{area}}$, $S2_{\text{area}}$), amplitude (QRS_{amp} , $S1_{\text{amp}}$, $S2_{\text{amp}}$), and morphology, obtained through principal component analysis (PCA), (QRS_{PCA} , $S1_{\text{PCA}}$, $S2_{\text{PCA}}$). The extracted features were resampled, filtered, and used in a regression framework to estimate respiratory flow and rate, validated against medical-grade reference systems. The results showed a moderate correlation ($r = 0.66$) between the estimated and reference respiratory waveforms [24]. Taken together, these findings indicate that respiration can influence both electrical and mechanical cardiac signals. Since CTIs are defined by the precise timing of these mechanical events, it becomes legitimate and methodologically relevant to question whether their estimation may also be affected by the respiratory phase, motivating the research hypothesis explored in the following section.

1.4 Research Hypothesis and Objectives

The present research is based on the hypothesis that certain CTIs may vary systematically throughout the respiratory cycle. Since several CTIs derive from the timing of heart sounds associated with valvular movements, it is reasonable to expect that intrathoracic pressure variations and respiration-induced changes in venous return could influence the temporal sequence of valve opening and closure. Although this possibility is physiologically intuitive, it requires experimental verification: the magnitude of the effect may be small, subject-dependent, or not readily detectable with non-invasive techniques. The aim of this study is therefore to conduct a pilot analysis to assess whether the respiratory phase measurably modifies CTIs estimated from ECG and PCG signals acquired with the device under investigation. Validating this hypothesis would clarify whether the integration of respiratory information enhances the robustness and interpretability of CTIs, and whether respiratory variability should be accounted for in future applications of the system.

1.5 Structure of the Thesis

The thesis is organized to guide the reader through the conceptual, technical and data-analysis steps that motivate and support the pilot investigation conducted in this work. The second chapter presents the State of the Art, offering an overview of the research that connects cardiac acoustic events, respiratory activity and the estimation of CTIs. The reviewed literature spans from early foundational studies to recent developments. Most contributions fall within the last fifteen years, approximately between 2010 and 2025, which represent the period in which digital phonocardiography, wearable monitoring and multimodal acquisition systems have evolved most rapidly. A further group of works published between 2000 and 2010 is included to capture the transition from traditional physiological investigations to the first algorithmic and sensor-based approaches for ECG-PCG analysis and accelerometry-derived respiration. Earlier studies from the 1950s to the 1970s, although considerably older, are retained as they constitute milestones in defining the physiological mechanisms underlying heart sound generation, the hemodynamic determinants of S_1 and S_2 and the respiratory modulation of valvular timing. The chapter therefore reflects both the historical progression and the current research focus in the field. Building on this background, the third chapter describes the experimental framework adopted in this study. The wearable multimodal device used for ECG, PCG and accelerometric acquisition is presented together with the data collection protocol, establishing the technical context required to interpret the subsequent analyses. The chapter also details the rationale behind the selected recording configuration and the characteristics of the subject population. The fourth chapter outlines the signal processing methods employed to extract respiratory information and

cardiac features from the collected data. The structure follows a progressive logic: first, the procedures specific to each signal modality are presented; then, a unified processing pipeline is introduced to harmonize the different respiratory estimates before their use in the phase-based analysis of cardiac latencies. This organization allows the reader to appreciate both the distinct physiological origins of the signals and the methodological coherence adopted in the study. The fourth chapter presents the results of the analysis, beginning with the evaluation of respiratory rate estimation across methods and followed by the assessment of CTIs under global and respiration-conditioned conditions. The chapter is structured to mirror the sequence of hypotheses tested, enabling a direct comparison between the different extraction and classification strategies. Finally, the fifth chapter discusses the findings in relation to the initial research hypothesis and the broader literature, identifying the methodological and physiological factors that may explain the observed behavior of CTIs. The concluding chapter summarizes the implications of the pilot study, outlines the limitations inherent to the current design and proposes directions for future work aimed at validating and extending the present findings.

Chapter 2

State of the Art

2.1 ECG and PCG in Cardiac Monitoring

ECG and PCG provide complementary information on the cardiac cycle, capturing respectively the electrical activation of the myocardium and the mechanical vibrations generated during valve motion [26,27]. The combined acquisition of the two signals enables a precise electro-mechanical alignment, which is essential for locating the timing of S_1 and S_2 and for deriving CTIs. Physiologically, S_1 follows the onset of ventricular depolarization after approximately 40–60 ms, while S_2 appears near the end of repolarization, reflecting the temporal correspondence between electrical activity and valve closure [28]. Several studies have demonstrated that ECG-PCG integration allows the extraction of systolic time intervals with values consistent with established physiological ranges. Klum et al. [24] validated a wearable system capable of jointly acquiring electrical and mechanical cardiac signals, reporting mean estimation errors of 10% for LVET and 21% for PEP (reduced to 7% and 16% in lateral positions) over more than 20 000 heartbeats. In addition, recent work [29] based on synchronized ECG and PCG recordings reported average EMAT, PEP, LVET and left ventricular systolic time (LVST) values of 74.35 ms, 89.00 ms, 244.39 ms and 258.60 ms, respectively, all consistent with reference standards. The same study found Q- S_1 and R- S_1 delays of 40.45 ms and 14.09 ms, closely matching the expected physiological values of approximately 45 ms and 15 ms, confirming the reliability of electro-mechanical alignment for identifying valve events. Altogether, these findings indicate that only the joint analysis of ECG and PCG provides access to timing parameters such as PEP, LVET and EMAT, which characterize ventricular performance and valve dynamics and cannot be derived from either modality alone. Building on this evidence, the following section examines the detection of individual heart sounds and computational approaches for estimating CTIs.

2.2 Detection of Heart Sounds and Estimation of CTIs

The main heart sounds, S_1 and S_2 , are generated by mechanical vibrations produced by the cardiovascular system [30–33]. These vibrations primarily result from the closure of the heart valves, events driven by pressure variations between the different cardiac chambers, but may also reflect myocardial wall contraction and blood flow turbulence within the great vessels [34]. The origin of S_1 and S_2 derives from the combination of multiple valvular components. The first sound is produced by the closure of the atrioventricular valves, mitral and tricuspid, occurring at the onset of ventricular systole when the intraventricular pressure exceeds the atrial pressure. The second sound consists of aortic and pulmonary components, corresponding to the asynchronous closure of the semilunar valves. This event takes place at

the onset of diastole, when ventricular pressure drops below that of the aorta and pulmonary artery [35]. Respiration modulates the timing of valve closure. Previous studies have shown that the timing of S_1 increases during inspiration and decreases during expiration, while S_2 exhibits a physiological respiratory split, typically ranging from 20 ms during expiration to approximately 50 ms during inspiration [35]. These findings confirm that respiratory-induced variations in mechanical valve events must be taken into account when extracting CTIs. A variety of approaches for heart sound detection has been proposed in the literature, including time–frequency analyses (such as STFT, Wigner–Ville and related distributions [35]) and model-based methods. Among these, envelope-based techniques represent one of the most established strategies for identifying S_1 and S_2 . One of the earliest and most widely cited methods was proposed by Liang et al. [36], who showed that the heart sound envelope enables reliable identification of S_1 and S_2 and allows the extraction of timing-related features such as peak location, duration and S_2 splitting. These findings support the use of envelope-based methods for timing analysis and provide the basis for the segmentation strategy adopted in this work. In this study, the Shannon envelope is used to segment heart sounds and extract the temporal landmarks required for CTIs computation.

2.3 Wearable ECG-PCG Devices for Cardiac Monitoring

The growing need for continuous and non-invasive monitoring of cardiovascular diseases has driven the development of a wide range of wearable devices that integrate ECG and PCG sensing for synchronized multimodal acquisition. To date, few studies have explored the use of ECG systems with closely spaced electrodes to obtain standard leads [37]. In a work by Lee et al. [28], the feasibility of a 12-channel ECG based on this configuration has been demonstrated. Building on this concept, Klum et al. [24] developed a wearable digital stethoscope patch integrating a single-lead ECG and impedance pneumography, with an inter-electrode distance of 55 mm. The reconstructed ECG was used to classify fiducial points and the S_1 and S_2 heart sounds acquired by the stethoscope, allowing the estimation of PEP and LVET over more than 20 000 heartbeats. Several recent works have investigated alternative sensor technologies for wearable heart sound acquisition, including piezoresistive MEMS arrays, piezoelectric elements, flexible substrates and fiber-optic solutions. Monteiro et al. [38] proposed a system combining electret microphones and dry polymer electrodes for the joint detection of ECG and PCG. More recently, Cho et al. [39] introduced a wearable device capable of recording both signals in parallel, although electret microphones may introduce limitations in signal fidelity. In Zang et al. [2], the authors presented a cost-effective solution based on PZT sensors, enabling real-time acquisition of ECG and PCG and the extraction of parameters such as EMD, LVET and PEP. Taken together, these developments highlight the growing technological potential of wearable ECG–PCG systems for integrated cardiac timing analysis.

2.4 Approaches to Respiratory Signal Estimation

The assessment of respiration plays a fundamental role in the diagnosis and management of cardiorespiratory diseases [40]. A significant example is the postoperative period, during which respiratory rate can serve as an early indicator of critical events, such as the onset of heart attack [41]. Traditionally, this evaluation has been performed through the direct observation of thoracic and abdominal movements by healthcare personnel, which

increases the margin of error and operational costs [40, 42, 43]. Although electronic methods for respiratory monitoring are now available, they often require the use of obstructive devices such as facial masks or nasal cannulas, which can compromise patient comfort and alter the natural breathing pattern. To overcome these limitations, several studies have highlighted the potential of accelerometers as alternative sensors for respiratory signal extraction [42–47]. These devices allow for continuous and non-invasive measurement of respiratory activity while preserving the natural physiology of breathing, an aspect particularly relevant for patients in vulnerable clinical conditions [43, 44]. Various methods have been developed to estimate respiratory activity using both mechanical and physiological signals. Among them, accelerometer-based approaches provide information on thoracic motion, while biosignal-based methods exploit respiration-induced modulations of cardiovascular signals. The following sections summarize the main developments in these two research domains.

2.4.1 Respiration Estimation from Accelerometric Signals

Among the earliest approaches to non-invasive respiratory monitoring, accelerometers were employed to capture thoracic motion associated with breathing. Hung et al. [48] proposed a method for estimating respiratory rate under static conditions using a biaxial sensor. This approach was later extended to the use of triaxial accelerometers, introducing a method based on hybrid PCA to improve the representation of respiratory movements [49]. However, these spatial acceleration-based methods present significant limitations due to motion artifacts and posture changes, as the acceleration signals induced by movement tend to mask the respiratory component. To overcome these limitations, Liu et al. [50] subsequently proposed a method capable of continuously estimating the breathing waveform, and thus the respiratory rate, even under dynamic conditions, by measuring inclination and variations in thoracic angle during activities characterized by different levels of energy expenditure (EE), such as walking, running, sitting, and sleeping. This approach, based on spectral analysis of the accelerometric signal, demonstrated greater robustness and resilience to artifacts compared to previous methods. Building on these findings, more recent studies have highlighted the benefits of using the accelerometric magnitude for respiration estimation. In particular, the sum vector of the three acceleration axes has been shown to improve sensitivity to chest expansion and contraction and to reduce the dependence on posture, providing a more stable representation of the respiratory waveform [51]. These findings support the use of norm-based approaches for continuous respiratory monitoring and justify the strategy adopted in this work, where the respiratory signal is derived from the vector magnitude of the sternum-mounted accelerometer.

2.4.2 Respiration Estimation from Biosignals

In addition to mechanical measurements, respiratory information can also be extracted from physiological signals that reflect cardiorespiratory interactions. Among these, the ECG is particularly relevant, as respiration induces characteristic modulations in both electrical and mechanical cardiac activity. These modulations can be exploited to estimate a respiratory waveform or breathing rate without the need for dedicated respiratory sensors. Respiratory signals can be extracted from ECG signal using either feature-based or filter-based techniques. The influence of respiration on these signals can be classified into three distinct types of modulation [52]:

- **Baseline wander (BW):** In the ECG, this component arises from variations in thoracic impedance and shifts in the electrical axis of the heart relative to the electrodes.

- **Amplitude modulation (AM):** During inspiration, the reduction in venous return leads to a decrease in stroke volume and, consequently, a reduction in the amplitude of the QRS complex in the ECG.
- **Frequency modulation (FM):** This modulation originates from RSA, a phenomenon in which HR increases during inspiration and decreases during expiration.

Charlton et al. [52] conducted a systematic study to analyze how technical and physiological factors influence the quality of respiratory signals extracted from ECG. The main objective was to assess the reliability of the three types of modulation (AM, FM, and BW) in reconstructing a respiratory signal and estimating respiratory rate across different contexts. The results showed that the quality of the extracted signal depends on several physiological factors, such as age or the presence of arrhythmias. In particular, FM was found to be less reliable in elderly subjects, as RSA tends to diminish or disappear with age. Moreover, the authors observed that the quality of most respiratory signals decreases at higher respiratory rates, indicating a general decline in estimation accuracy. The study therefore emphasized that the robustness of extraction techniques is strongly dependent on the subject's physiological condition and the measurement context.

The evidence that respiration induces measurable amplitude, baseline and frequency modulations in the ECG signal supports the use of ECG-derived features for respiratory estimation. For this reason, ECG-based respiration was included among the methods adopted in this study, in addition to the accelerometric approach.

2.5 Effect of Respiratory Phase on CTIs Accuracy

It is essential to understand the physiological effects of respiration on heart sounds, as the pressure and volume variations, induced by the respiratory cycle, influence both the morphology and timing of cardiac mechanical events. Variations in heart sounds reflect the influence of respiration on the timing of cardiac valve closure, mediated by changes in intrathoracic pressure and venous return dynamics, which affect ventricular filling. During inspiration, the reduction in intrathoracic pressure caused by the expansion of the thoracic cavity promotes blood flow to the right ventricle, resulting in delayed closure of the pulmonary valve and earlier closure of the aortic valve. This phenomenon leads to an increase in the splitting of the second heart sound. During expiration, the opposite process occurs: venous return decreases and the two components tend to merge [35]. The physiological split of the second heart sound thus serves as an indicator of the hemodynamic variations that occur throughout the respiratory cycle. Regarding the first heart sound, the study conducted by Tang et al. (2015) [34] showed that the delay in S_1 progressively increases during inspiration, reaching its maximum at the end of this phase, and decreases during expiration. Respiratory-induced variations in the preload and afterload of the ventricular affect the temporal relationship between electrical activation and the mechanical response of the myocardium, altering both the morphology and timing of heart sounds. In a quantitative study modeling heart sounds as a sum of Gaussian curves, morphological variations were analyzed in terms of amplitude, timing, and supporting width. The amplitude of S_2 was found to increase during inspiration and diminish during expiration, while no consistent trend was observed for S_1 . Additionally, the supporting width of S_1 increased during inspiration and decreased during expiration, reflecting the mechanical impact of intrathoracic pressure fluctuations on valve dynamics. The delay span of S_2 was often found to be greater than that of S_1 , suggesting that respiratory activity exerts a stronger modulation on the mechanical events associated with semilunar valve closure. These cyclic morphological changes confirm the high sensitivity of cardiac sounds to respiration-induced hemodynamic

variations, providing a non-invasive window into cardiorespiratory coupling [53]. Several studies have quantified the influence of respiration on CTIs. In the classic work by Nandi et al. [54], heart rate remained stable between inspiration (73.2 ± 14.6 breaths per minute) and expiration (72.5 ± 14.0 breaths per minute), confirming that the observed variations in CTIs were not attributable to changes in cardiac rhythm. The PEP was significantly shorter at peak expiration than at peak inspiration ($p < 0.05$), with most of the inspiratory increase occurring by mid-inspiration; beyond this point, the variation was minimal (mean difference 0.63 ms). Conversely, LVET was significantly longer at mid-expiration than at peak inspiration ($p < 0.005$), and most of the inspiratory shortening occurred by mid-inspiration ($p < 0.001$). These results demonstrate that respiration systematically modulates both PEP and LVET, with inspiration increasing PEP and reducing LVET, while expiration produces the opposite effect. Such phase-dependent variations highlight the importance of accounting for respiratory dynamics when estimating CTIs. This behavior can be explained by the decrease in pleural pressure that occurs during inspiration, which leads to a relative increase in aortic pressure and, consequently, in afterload. This effect causes a delay in mitral valve closure and aortic valve opening, thereby prolonging PEP. During expiration, the opposite process occurs: reduction in afterload shortens PEP and prolongs ejection time [55]. These findings confirm that respiration-induced hemodynamic variations affect the timing of mechanical cardiac events and, as a result, may compromise the accuracy of CTIs estimation.

2.6 Open Challenges in the Interaction Between Respiratory and Cardiovascular Signals

Interactions between the respiratory and cardiovascular systems represent a complex and dynamic phenomenon, still under investigation due to its nonlinear nature and the challenges associated with accurate modeling. Respiratory modulations simultaneously affect electrical, mechanical, and hemodynamic parameters of the heart, leading to variations in frequency, morphology, and timing of cardiac events. However, the cardiorespiratory response exhibits high interindividual variability and depends on several factors, such as respiratory rate, breath depth, and the subject's autonomic state. This complexity makes it difficult to isolate the direct effects of respiration on cardiovascular signals and poses a significant challenge for the quantitative analysis and modeling of heart-lung coupling. Although recent studies have demonstrated the feasibility of estimating respiratory and cardiac parameters using non-invasive devices based on biosignal acquisition, several challenges remain in ensuring robust and reliable monitoring of cardiorespiratory interactions in real-time and over extended periods. One of the main limitations is the presence of motion artifacts, which inevitably degrade signal quality. Body movements, postural changes, or even speech, difficult to control in a home environment compared to experimental settings, can introduce non-physiological fluctuations that obscure subtle respiratory modulations, leading to erroneous segmentation of mechanical events and, consequently, inaccurate estimation of CTIs. Another critical issue arises from irregular heart rhythms, such as arrhythmias, which introduce additional variability and pose significant challenges to algorithms based on regular beat-to-beat cadence. The normal physiological coupling between respiration and cardiac dynamics may thus be disrupted, reducing the coherence of features that depend on the respiratory phase. This variability affects the accuracy and robustness of CTIs estimation, particularly when the timing of mechanical valve events is influenced by irregular rhythms, motion artifacts or rapid changes in intrathoracic pressure. The impact of such variability on the accuracy and robustness of respiration-dependent CTIs estimation remains an open question, particularly regarding the system's adaptability to different physiological conditions. Addressing these challenges requires careful signal preprocessing

and artifact management, as well as robust strategies for combining information from accelerometry, ECG and PCG. In this context, methods based on multimodal acquisition and cardiac timing estimation represent a promising direction for improving the reliability of non-invasive home-based monitoring systems [24].

Chapter 3

Materials and Methods

3.1 Description of the Wearable Device

The wearable system used in this study was specifically developed to enable the simultaneous acquisition of ECG, PCG, and accelerometric signals. The multimodal configuration was designed to investigate the interaction between electrical, mechanical, and acoustic cardiac activity, while also extracting respiratory information from chest motion. The core component of the device consists of a flexible array that conforms to the subject's left hemithorax as shown in Figure 3.1. The array integrates 48 electret condenser microphones (4 mm diameter) for PCG acquisition, homogeneously distributed over a grid, with 16 mm spacing between adjacent elements and three electrodes for single-lead ECG recording. This dense spatial distribution ensures adequate coverage of the left thoracic surface and enables users with no prior experience in auscultation to perform high-quality recordings without assistance from clinical or technical personnel. Signals are pre-amplified onboard and acquired, along with the ECG, through a commercial I/O device (NI USB-6210, National Instruments[®]) that performs analog-to-digital conversion at 1 kHz and transfers the data to a personal computer. The array is flexible to adapt to the chest surface [56, 57]. A miniaturized magneto-inertial measurement unit (MIMU) is positioned on top of the array, over the sternal area, to capture 3D chest wall accelerations, allowing the detection of both cardiac-induced microvibrations and respiratory-induced movements. The inertial data are processed by an onboard floating-point microcontroller.

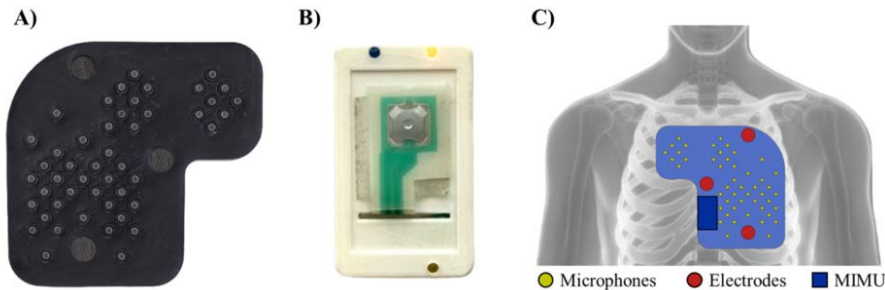


Figure 3.1: Configuration of the acquisition system. A) Setup for ECG and PCG signal collection. B) Inertial sensor (MIMU) for measuring chest wall accelerations. C) Placement of the sensing elements on the thoracic surface [58].

3.2 Data Acquisition Protocol

Twelve healthy volunteers (5 females) participated in the data acquisition sessions. All participants reported no history of cardiovascular or respiratory diseases and no ongoing medication that could influence cardiac or respiratory activity. Healthy subjects were included to allow a preliminary evaluation of whether respiratory signal analysis could improve the accuracy of CTIs estimation. Each participant was fitted with the acquisition device using an adjustable vest-like support belt designed to ensure stable sensor positioning according to individual body shape. Data were collected with subjects lying in a supine position on an examination bed, instructed to remain still and breathe spontaneously without any imposed rhythm or verbal cue, to preserve natural respiratory patterns. The recordings were performed under conditions representative of a typical home monitoring, without controlled environmental conditions, to ensure measurement validity. For each subject, a single recording of 60 seconds was acquired. The participants had a median age of 25 years (range: 24–70 years). Detailed anthropometric characteristics are listed in Table 3.1. Although the sample size is limited, the study can be regarded as a pilot investigation aimed at assessing the feasibility and consistency of the proposed approach. Recordings from two participants were excluded due to excessive ECG noise, yielding a final dataset of ten subjects.

Table 3.1: Anthropometric characteristics of the participants.

| Subject ID | Age | Gender | Height (m) | Weight (kg) | BMI (kg m ⁻²) |
|------------|-----|--------|------------|-------------|---------------------------|
| subj_01 | 30 | F | 1.70 | 69 | 23.9 |
| subj_02 | 27 | F | 1.70 | 58 | 20.07 |
| subj_03 | 70 | M | 1.77 | 76 | 24.3 |
| subj_04 | 25 | M | 1.83 | 83 | 24.8 |
| subj_05 | 25 | F | 1.67 | 55 | 19.7 |
| subj_06 | 24 | M | 1.90 | 90 | 24.9 |
| subj_07 | 28 | F | 1.60 | 50 | 19.5 |
| subj_08 | 24 | M | 1.80 | 70 | 21.6 |
| subj_09 | 26 | M | 1.76 | 71 | 22.9 |
| subj_10 | 24 | M | 1.74 | 59 | 19.5 |
| subj_11 | 25 | F | 1.64 | 66 | 24.5 |
| subj_12 | 25 | M | 1.78 | 71 | 22.4 |

3.3 Methods for Estimating the Respiratory Signal

Respiratory information was estimated from three physiological signals recorded simultaneously: acceleration, ECG, and PCG. The hypothesis is that these signals contain respiration-related components arising from distinct physiological mechanisms, such as mechanical chest wall motion in the acceleration signals, RSA in the ECG, and variations in cardiac sounds in the PCG. To minimize transient artifacts, the initial second of each recording was excluded from analysis, as identified through visual inspection of the dataset. Signal-specific methods were implemented to extract respiratory information from each modality. This section describes the signal-specific extraction procedures (Sections 3.3.1–3.3.4) and the shared processing steps used to obtain the final respiratory waveforms (Section 3.3.5). All processing routines were implemented in MATLAB R2023b (The MathWorks, Natick, MA, USA).

3.3.1 Accelerometer-derived respiration

The respiratory signal was derived from the triaxial accelerometer positioned on the sternum, which captures the mechanical expansion and contraction of the thoracic wall during breathing. Prior to processing, the mean of each acceleration axis was removed to eliminate the direct current (DC) component. The three acceleration components were combined into a single magnitude signal by computing the Euclidean norm:

$$a_{\text{norm}}(t) = \sqrt{a_x^2(t) + a_y^2(t) + a_z^2(t)}. \quad (3.1)$$

The use of the vector norm, rather than a single-axis signal, was preferred as it improves the sensitivity of the device in capturing chest wall motion due to respiration [51]. This approach is consistent with the findings of Lin and Jhou [59], who applied wavelet analysis to extract respiratory frequency from seismocardiogram signals recorded by MEMS triaxial accelerometers in a supine posture, achieving a very low estimation error of 0.0035 ± 0.0628 Hz (0.21 ± 3.77 breaths per minute (bpm) in respiratory rate). These results confirm the feasibility of estimating respiratory rate from accelerometric signals under controlled postural conditions. Furthermore, previous studies have shown that no significant differences are typically observed among orthogonal acceleration directions, supporting the use of combined-axis representations to improve robustness across varying postures and sensor placements [60]. The resulting norm signal was then downsampled to 25 Hz to reduce computational load before the application of the subsequent processing steps described in Section 3.3.6. The preprocessing workflow is illustrated in Figure 3.2.

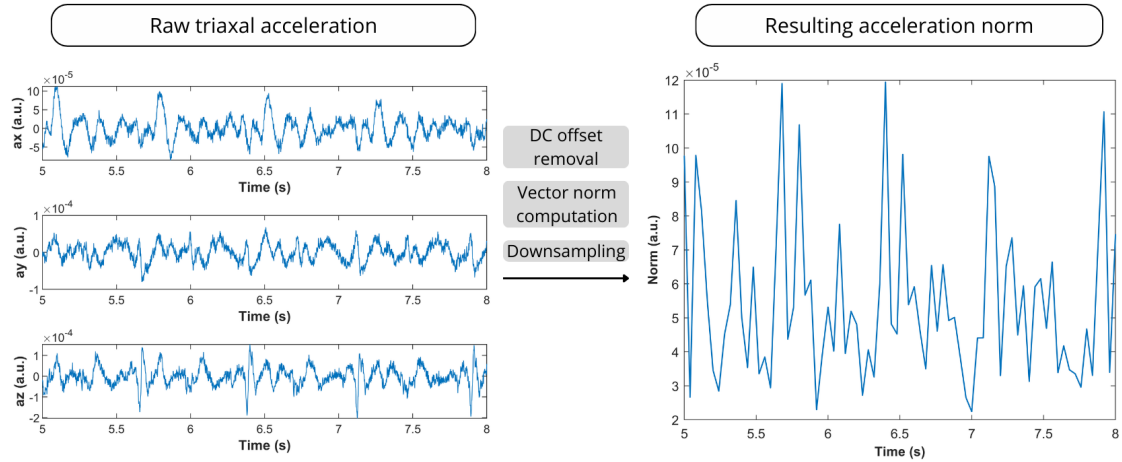


Figure 3.2: Preprocessing of the triaxial accelerometer signal. The raw acceleration along the three axes was corrected for DC offset, combined into a single waveform through the Euclidean norm, and downsampled to obtain the resulting acceleration norm.

3.3.2 ECG-derived respiration

Accurate R-peak detection is essential to ensure the reliability of the continuous respiratory signal reconstructed from the ECG. In this work, R-peak detection was performed using a publicly available on the MATLAB file exchange implementation [61] of the Pan–Tompkins algorithm rather than the original formulation described in [62]. The adopted implementation does not include all the elements of the original decision logic, in particular the dual-threshold mechanism and the associated refractory control in the adaptive thresholding stage. Because of this, additional criteria were introduced to improve robustness under

the specific characteristics of the data acquired with our device, which uses a non-standard single-lead ECG configuration. In particular, the algorithm was refined through: (i) enforcement of a minimum refractory period of 0.35 s to prevent multiple detections within the same cardiac cycle, by retaining the candidate with the highest combined score based on amplitude and slope; and (ii) exclusion of low-amplitude detections below 30% of the median R-peak value. A refractory period of 350 ms was set to avoid spurious double detections within the same cardiac cycle. This choice also accounts for the possibility that, in our non-standard lead configuration, the T wave may exhibit relatively large amplitude, thereby increasing the risk of misclassifying it as an additional R peak. Although 200 ms represents the physiological lower limit for RR intervals [63], a longer interval was adopted here to improve detection robustness in noisy segments, while still accommodating all physiologically plausible heartbeats under resting conditions. Parameter values were empirically determined through inspection of the acquired ECG recordings. These modifications are illustrated in Figure 3.3, which compares the original implementation (A) with the modified version (B). The refined algorithm effectively removes false detections occurring within the same cardiac cycle, thereby improving the robustness of R-peak identification. The resulting sequence of R-peak locations was then used to derive two respiratory signals, reflecting on temporal and morphological modulations of the ECG.

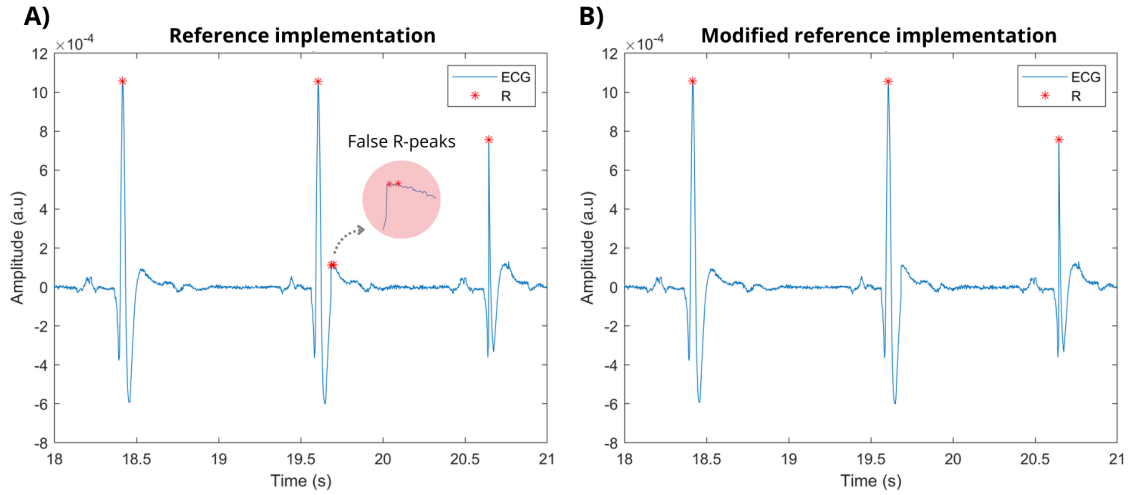


Figure 3.3: Comparison between the reference (A) and modified (B) algorithms for R-peak detection, with the modification enforcing a 0.35 s refractory period and an amplitude–slope criterion to retain the most representative peak, thereby preventing false multiple.

RR-based extraction

The first respiratory estimate was obtained from the beat-to-beat variability of the cardiac period. Consecutive R–R intervals were computed from the sequence of detected R-peaks, and the resulting series was interpolated to yield a continuous respiratory waveform with uniform sampling. This approach exploits the well-known coupling between respiration and heart rate, known as RSA, whereby breathing modulates cardiac cycle length. Figure 3.4 illustrates the detection of consecutive R–R intervals from the ECG signal, highlighting the identified R-peaks and the computation of the temporal distance between successive beats.

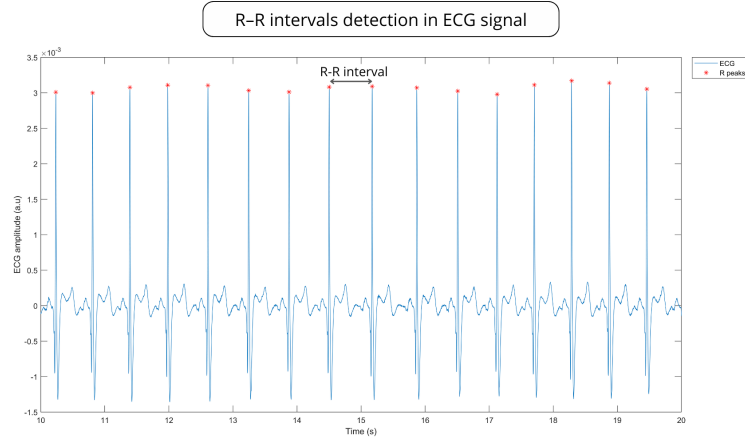


Figure 3.4: Detection of R–R intervals in the ECG signal. Consecutive R peaks (red markers) were identified using the modified Pan–Tompkins algorithm, and the R–R interval was computed as the temporal distance between successive peaks.

Amplitude-based extraction

A second respiratory estimate was derived from respiratory-induced modulations of the QRS complex amplitude, following the method proposed in [64]. For each detected R-peak, the corresponding S-wave was identified as the minimum value of the ECG within a 0.1 s window after the R-peak, enabling the computation of the R–S amplitude difference for each cardiac cycle, even when the S deflection was shallow or poorly defined. The resulting sequence of R–S amplitudes reflects respiration-related morphological variations of the ECG and was used to generate an additional respiratory waveform. Figure 3.5 illustrates the detection of R and S peaks in the ECG signal, highlighting the identified markers used to compute the respiratory signal through amplitude modulation.

Both ECG-derived discrete series were subsequently processed according to the steps described in Sections 3.3.5 and 3.3.6.

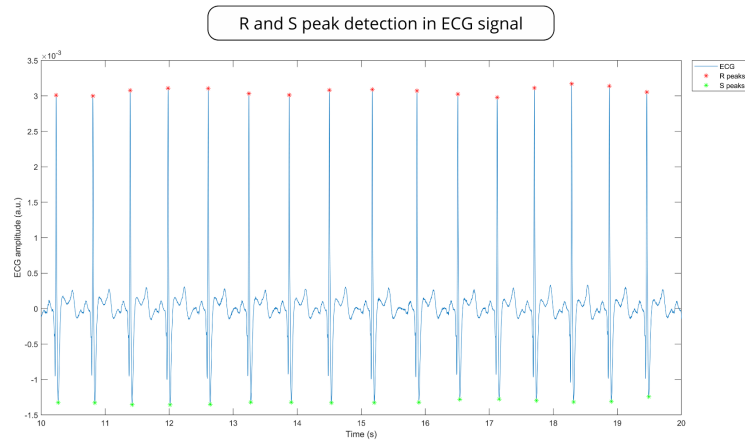


Figure 3.5: Detection of R and S peaks in the ECG signal. The positions of R peaks (red markers) and S peaks (green markers) were identified for the computation of the respiratory signal through amplitude modulation (AM).

3.3.3 PCG-derived respiration

Based on the physiological mechanisms underlying the generation of the S_1 and S_2 heart sounds (see Section 2.2), both components were analyzed to assess respiration-induced modulations in cardiac timing. The extraction was performed separately for S_1 and S_2 in order to evaluate which component provided a more robust respiratory estimate. All PCG channels were first band-pass filtered between 20 and 100 Hz using a fifth-order Chebyshev type II filter with a 20 dB stopband attenuation, implemented in zero-phase configuration. This frequency band was selected to isolate the main spectral components of heart sounds while minimizing noise and motion artifacts [65].

Quality metrics and channel selection

The SNR was, then, computed for each filtered channel following the formulation proposed in [66]. The SNR was defined as:

$$\text{SNR} = 20 \log_{10} \left(\frac{A_S}{4\sigma_N} \right), \quad (3.2)$$

where A_S represents the peak-to-peak amplitude of the mean cardiac cycle, and σ_N is the standard deviation of the noise estimated within the 70–85% portion of the mean cycle, where no heart sounds are expected.

Computing the SNR on the band-pass filtered signals ensured that channel selection reflected the actual heart-sound quality rather than broadband noise. The subsequent steps were applied exclusively to the selected channel. To enhance the signal-to-noise ratio and facilitate the precise identification of S_1 and S_2 peaks, the PCG envelope was computed using the second-order Shannon energy (SE) [66]:

$$\text{SE} = -\frac{1}{N} \sum_{i=1}^N x^2(i) \cdot \log x^2(i) \quad (3.3)$$

where x is the signal and N is the 20 ms integration window. Crucially, the window was shifted sample-by-sample to preserve the native 1 ms resolution required for subsequent latency estimation. To mitigate the dependency on signal quality variations along the recording, a moving normalization was applied to the Shannon energy using the mean and standard deviation computed over a 1 s sliding window. Negative values were subsequently set to zero to obtain a non-negative envelope while preserving the original 1 ms temporal resolution [66]. After filtering and envelope computation, the analysis proceeded by focusing separately on S_1 and S_2 , in order to assess which component provided a more stable and reliable respiratory estimate.

S_1 -based extraction

In the S_1 -based extraction, the analysis focused on the first heart sound, corresponding to the closure of the atrioventricular valves and occurring shortly after ventricular depolarization. For each cardiac cycle, S_1 peaks were identified within the first 20% of the R–R interval following each R-peak in the ECG. This temporal window is consistent with the expected timing of S_1 within the cardiac cycle and with classification criteria reported in previous studies [66]. The algorithm identifies one peak per cardiac cycle within the expected window. Occasional deviations in peak prominence do not substantially affect the derived respiratory signal, since subsequent interpolation and low-pass filtering stages suppress isolated inconsistencies and preserve the underlying respiratory trend. The sequence of detected S_1 events was used to compute the S_1 – S_1 intervals, which reflect respiration-induced variability in cardiac timing. These intervals constituted a discrete time series of respiration-dependent modulation of heart sound timing and were subsequently processed as described in Sections 3.3.5 and 3.3.6. Figure 3.6 illustrates the Shannon energy envelope

of the PCG signal from the selected channel and the identification of S_1 peaks within the expected temporal window following each R-peak.

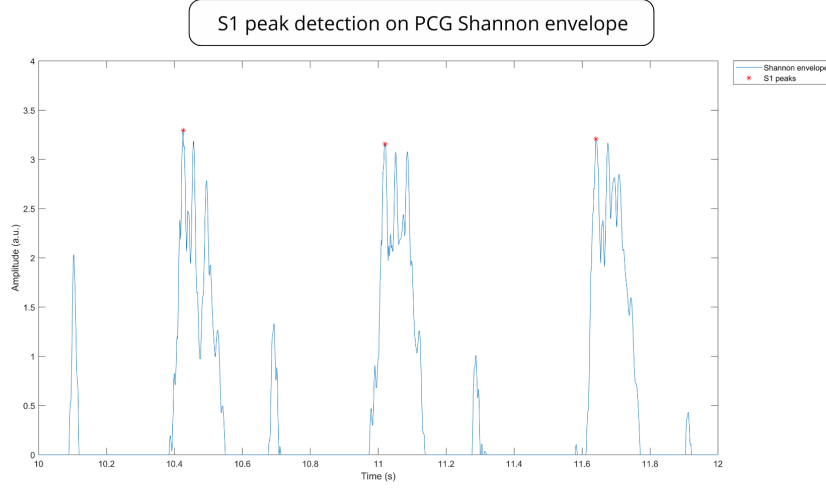


Figure 3.6: Shannon envelope of the PCG signal from the selected channel and identification of S_1 peaks.

S_2 -based extraction

A similar procedure was applied to extract the respiratory signal from S_2 , related to the closure of the semilunar valves. S_2 peaks were identified within the 30–60% portion, according to the expected temporal position of S_2 relative to the cardiac cycle, of each R–R interval, based on the corresponding ECG R-peak timing. For each PCG channel, the sequence of S_2 occurrences was used to compute the S_2 – S_2 intervals, capturing the respiratory influence on the temporal spacing of cardiac sounds. As in the S_1 -based extraction, one peak per cardiac cycle was identified within the defined window. The subsequent interpolation and filtering steps mitigated local irregularities, ensuring a stable respiratory waveform. The resulting interval series provided a discrete representation of the respiration-related variability in the timing of S_2 and was subsequently processed as detailed in Sections 3.3.5 and 3.3.6. Figure 3.7 illustrates the Shannon energy envelope of the PCG signal from the selected channel and the identification of S_2 peaks, located within the expected temporal window defined relative to the corresponding R-peak in the ECG.

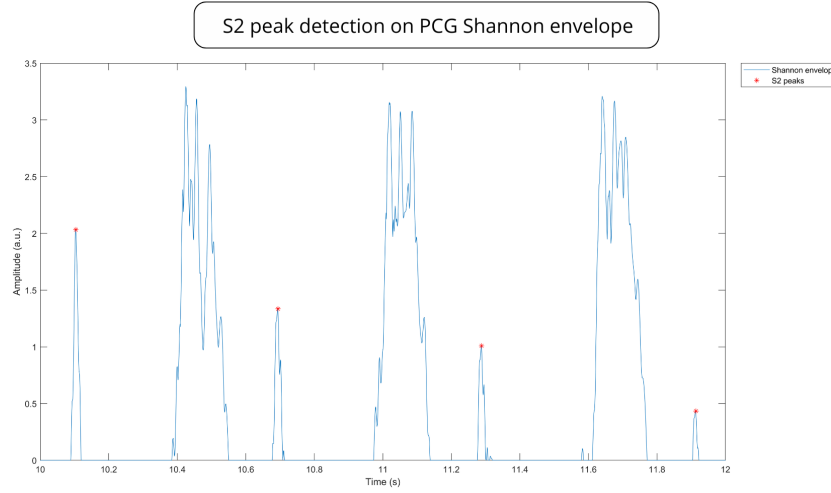


Figure 3.7: Shannon envelope of the PCG signal from the selected channel and identification of S_2 peaks.

3.3.4 Cardiac latency–derived respiration

The respiratory signal was also estimated from the beat-to-beat variations in the timing of cardiac valve events, quantified as the latencies between the R-wave of the ECG and the main heart sound components, namely the mitral (S_{1m}) and tricuspid (S_{1t}) components of S_1 , and the aortic (S_{2a}) and pulmonary (S_{2p}) components of S_2 . ECG and PCG signals were processed using algorithms previously developed and validated in [66]. Briefly, the ECG was band-pass filtered between 10 and 35 Hz through the cascade of two 250th-order FIR filters, a range that encompasses the main frequency content of the QRS complex. The delay introduced by FIR filtering was compensated to preserve the temporal alignment with the other signals. R-peaks were detected using a modified version of the Pan–Tompkins algorithm [67], as implemented in [66]. The PCG signals were band-pass filtered between 20 and 100 Hz using a fifth-order Chebyshev IIR filter applied in a zero-phase configuration. Heart sounds were segmented using the normalized second-order Shannon energy envelope described above in Section 3.3.3. To ensure the robust identification of valve components and the rejection of artifacts, a multi-stage detection logic was applied to this envelope. First, potential heart sound segments were identified based on an adaptive amplitude threshold (set to 5% of the maximum energy). Adjacent segments were merged if their separation was physiologically negligible to prevent the fragmentation of single sounds. Subsequently, the internal split within each segment was located as the deepest local energy minimum, allowing the separation of the first sound into mitral and tricuspid components, and the second sound into aortic and pulmonary components. Finally, false positives were removed by applying temporal constraints based from the R-R interval, ensuring that detected peaks were consistent with physiological cardiac timing [66]. For each cardiac cycle, the temporal latencies between the R-wave and the corresponding valvular components were computed and subsequently converted from milliseconds to seconds to ensure unit consistency across all derived signals. The resulting beat-to-beat latency series provided a discrete representation of respiration-related variability and were subsequently processed as detailed in Sections 3.3.5 and 3.3.6. For illustrative purposes, the Shannon envelope was computed from the channel providing the best detection of S_1 (Figure 3.8) and from the channel providing the best detection of S_2 (Figure 3.9). Distinct temporal windows were selected to highlight the respective valve components relative to the R-peaks of the ECG.

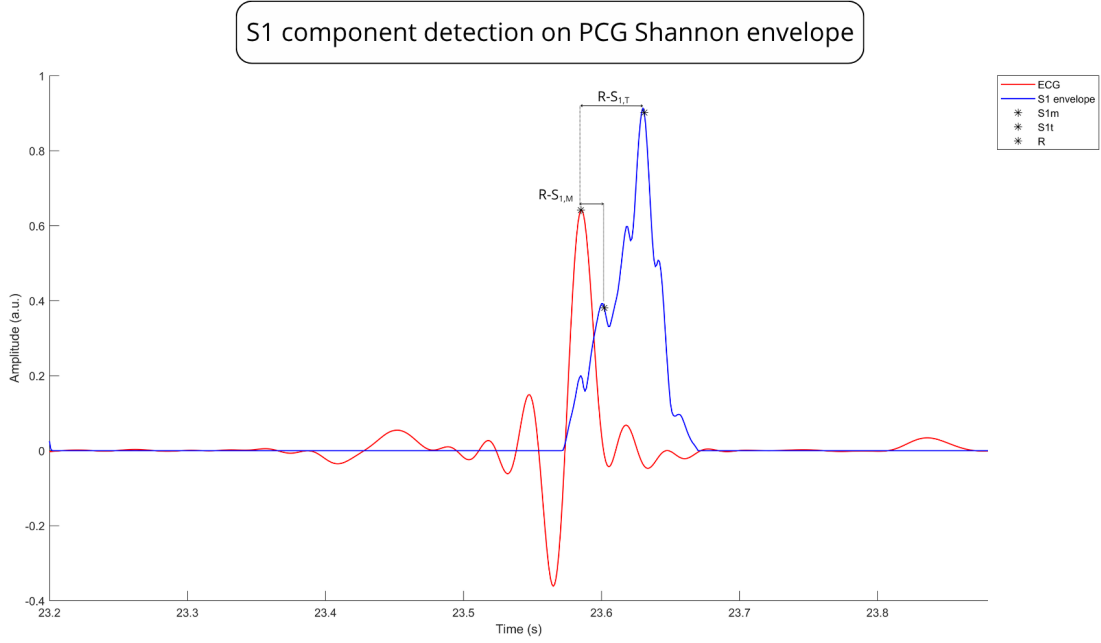


Figure 3.8: Detection of the S_{1m} and S_{1t} components of S_1 on the Shannon envelope of the PCG signal, synchronized with the ECG trace and the corresponding R peaks.

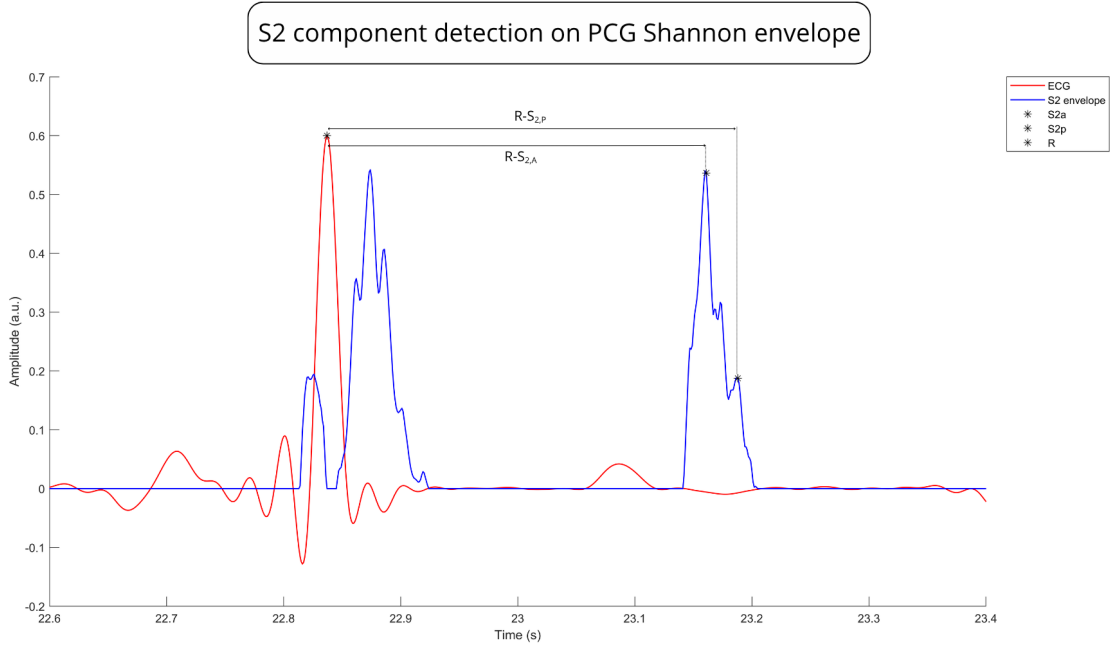


Figure 3.9: Detection of the S_{2a} and S_{2p} components of S_2 on the Shannon envelope of the PCG signal, aligned with the ECG trace and the corresponding R peaks.

3.3.5 Interpolation of discrete respiratory estimates

All respiratory estimates derived from cardiac information, namely the RR-based, amplitude-based, S_1 -based, S_2 -based, and valve-latency-based series, were obtained as beat-to-beat,

nonuniformly sampled time sequences. Prior to the processing stages described in Section 3.3.5, all discrete series were interpolated onto a uniform time base of 25 Hz to obtain continuous respiratory waveforms suitable for comparison across modalities. The piecewise cubic Hermite interpolation (pchip) method was adopted after evaluating commonly used schemes for physiological signals. Linear interpolation avoids oscillatory artifacts but may introduce slope discontinuities, whereas spline interpolation ensures smoothness at the cost of overshooting and generating artificial extrema. In contrast, pchip preserves the monotonicity and overall shape of the original data without introducing spurious oscillations, thereby providing physiologically consistent respiratory waveforms and reliable reconstruction of respiratory cycle boundaries.

3.3.6 Common Processing Pipeline

After bringing all respiratory estimates to a uniform sampling frequency of 25 Hz, a common processing pipeline was applied to ensure physiologically consistent continuous respiratory waveforms and temporal alignment across modalities. A zero-phase low-pass Chebyshev type II filter of seventh order was applied, with a stopband attenuation of 50 dB and a normalized cutoff frequency of 0.5 Hz consistent with the typical frequency range of respiration (0.1–0.6 Hz) observed in adults under different body activities [50]. To ensure that the filtering stage effectively removed the cardiac component regardless of individual variability in heart rate, the average heart rate was computed for each subject from the R-peaks identified in the ECG signals (see Section 3.3.4). The resulting heart rates ranged from approximately 49 to 94 beat per minute (i.e., 0.8–1.6 Hz), confirming that the selected cutoff frequency of 0.5 Hz lies well below the typical spectral content of the cardiac signal and is thus adequate to isolate the respiratory component across all subjects. This filtering stage preserved the morphology of the respiratory waveform while reducing high-frequency fluctuations and residual cardiac component. A 10 s moving average was then applied and subtracted from each respiratory estimate to remove slow baseline trends and low-frequency fluctuations unrelated to breathing. The window length was selected to effectively suppress very slow variations while maintaining the typical frequency content associated with normal respiratory activity in healthy awake adults at rest. This operation further mitigates low-frequency variations arising from slow postural adjustments, mechanical instabilities, or gradual physiological changes that can introduce non-respiratory modulations across all sensing modalities. The resulting signals represent the continuous respiratory waveforms derived from each source, used for all subsequent analyses and comparisons. Figure 3.10 illustrates the step-by-step application of the common processing pipeline using the acceleration signal as a reference example. This signal was selected for visualization purposes, as it directly reflects thoracic motion and serves as the respiratory reference throughout the study. Respiratory rate was then estimated for each signal as the inverse of the average cycle duration, computed from the interval between successive inspiratory onsets detected by the ZC-AT algorithm described in the following section. This yielded a global respiratory rate in bpm, allowing comparison across modalities.

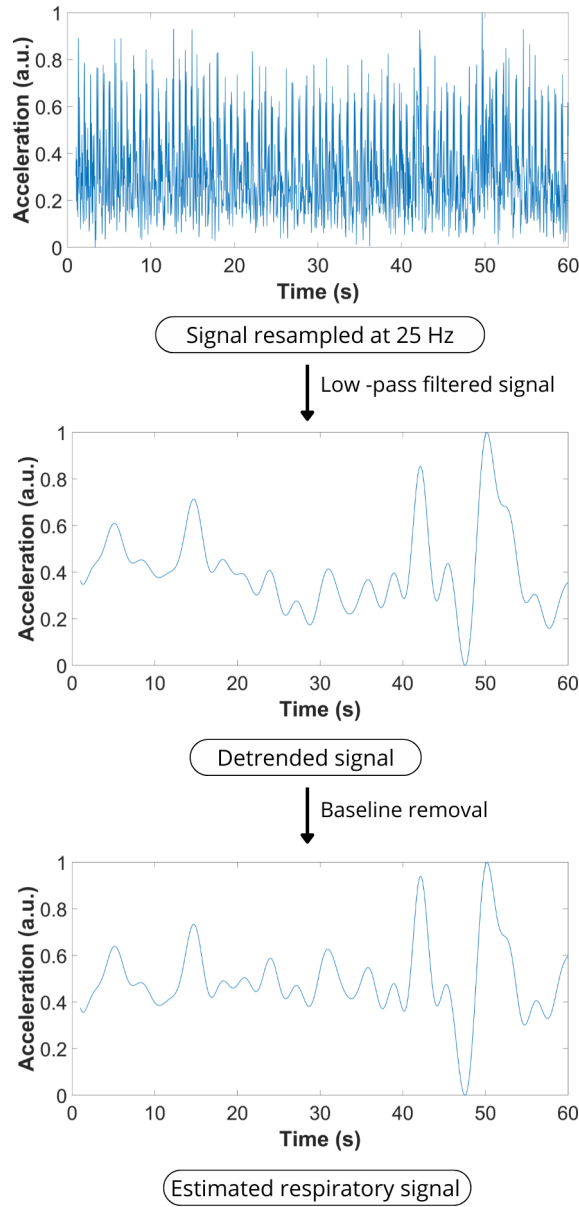


Figure 3.10: Processing pipeline applied to the norm of the acceleration signal, used as the respiratory reference.

3.4 Identification of Respiratory Phases and Characteristic Points

The segmentation of the respiratory signal into inspiratory and expiratory phases was performed by identifying local maxima and minima using a Zero-Crossing with Amplitude Threshold (ZC-AT) algorithm derived from Khodadad et al. [68]. The algorithm analyzes the zero-crossings of the signal to alternately detect end-expiration points (minima) and end-inspiration points (maxima). Specifically, the algorithm alternates between two detection phases depending on the type of zero-crossing encountered. When the most recent

zero-crossing is falling, meaning the signal transitions from positive to negative, it initiates a minimum detection phase (end of expiration). Conversely, when the crossing is rising (from negative to positive), it initiates a maximum detection phase (end of inspiration). This approach enforces an alternating sequence of minima and maxima, referred to as Waiting for Rising Crossing (WRC) and Waiting for Falling Crossing respectively (WFC), ensuring physiological plausibility and temporal consistency between respiratory cycles. Each potential extremum is validated based on two temporal criteria: the interval between consecutive crossings with the same slope, defined as Identical Crossing Spacing (ICS), and the interval between consecutive crossings with opposite slopes, defined as Different Crossing Spacing (DCS). The extrema are accepted only if both intervals exceed minimum thresholds, namely Minimum Identical Crossing Spacing (MICS) and Minimum Different Crossing Spacing (MDCS), calculated as:

$$\text{MICS} = \text{MICS}_{\text{fact}} \cdot \frac{60}{\text{maxBR}}, \quad \text{MDCS} = \text{MDCS}_{\text{fact}} \cdot \frac{60}{\text{maxBR}}$$

where $\text{MICS}_{\text{fact}}$ and $\text{MDCS}_{\text{fact}}$ are dimensionless factors scaling the temporal thresholds relative to the maximum respiratory rate (maxBR), fixed at 150 breaths/min. This value was kept consistent with the original formulation of [68], where it serves as a theoretical limit for temporal normalization and does not represent a physiological value for adult subjects. To reduce false detections caused by small-amplitude oscillations or noise, an additional amplitude-based validation criterion was introduced. The minimum acceptance threshold, referred to as Low Tidal Amplitude (lowTA), is defined as:

$$\text{lowTA} = \text{typTA} \cdot \text{lowTA}_{\text{fact}}$$

where typTA (Typical Tidal Amplitude) represents the typical tidal amplitude, corresponding to the 80th percentile of the respiratory amplitude distribution, and $\text{lowTA}_{\text{fact}}$ is a coefficient between 0 and 1 defining the minimum fraction of the typical amplitude required for a cycle to be considered valid. The parameters $\text{MICS}_{\text{fact}}$, $\text{MDCS}_{\text{fact}}$, and $\text{lowTA}_{\text{fact}}$ were initially explored within the following validity ranges:

$$\text{MICS}_{\text{fact}} \in [0.5, 0.75], \quad \text{MDCS}_{\text{fact}} \in [0.1, 0.25], \quad \text{lowTA}_{\text{fact}} \in [0.1, 0.9]$$

The parameter configurations were considered acceptable only if they produced physiological respiratory rates for awake, resting adults (6–20 breaths/min) and at least five coherent respiratory cycles. respiratory rates within this range were considered physiologically plausible, as slower frequencies (6–11 breaths/min) that have been shown to enhance vagal power by entraining cardiac activity to the respiratory rhythm, thereby strengthening parasympathetic modulation [69], while typical spontaneous breathing in healthy adults falls between 12 and 20 breaths/min, with 90% of values reported within 11.8–19.2 breaths/min [70]. The analysis showed a stable convergence toward $\text{MICS}_{\text{fact}} = 0.50$ and $\text{MDCS}_{\text{fact}} = 0.10$, in agreement with the values originally proposed by [68]. The parameter $\text{lowTA}_{\text{fact}}$ exhibited greater variability, but the choice of 0.10 proved to be the most balanced, as it preserved the physiological plausibility of the respiratory rate while maintaining the inclusion of low-amplitude cycles. The final parameter values and their respective exploration ranges are reported in Table 3.2.

Table 3.2: Explored ranges and final values of the parameters used for respiratory signal segmentation.

| Parameter | Description | Explored range | Final value |
|----------------|--|----------------|-------------|
| $MICS_{fact}$ | Scaling factor for the ICS threshold | [0.5, 0.75] | 0.50 |
| $MDCS_{fact}$ | Scaling factor for the DCS threshold | [0.1, 0.25] | 0.10 |
| $lowTA_{fact}$ | Minimum fraction of the typical tidal amplitude required for a valid cycle | [0.1, 0.9] | 0.10 |

The detection logic is illustrated in Figure 3.11, where the alternation between states and the validation of candidate extrema are shown for both expiration and inspiration.

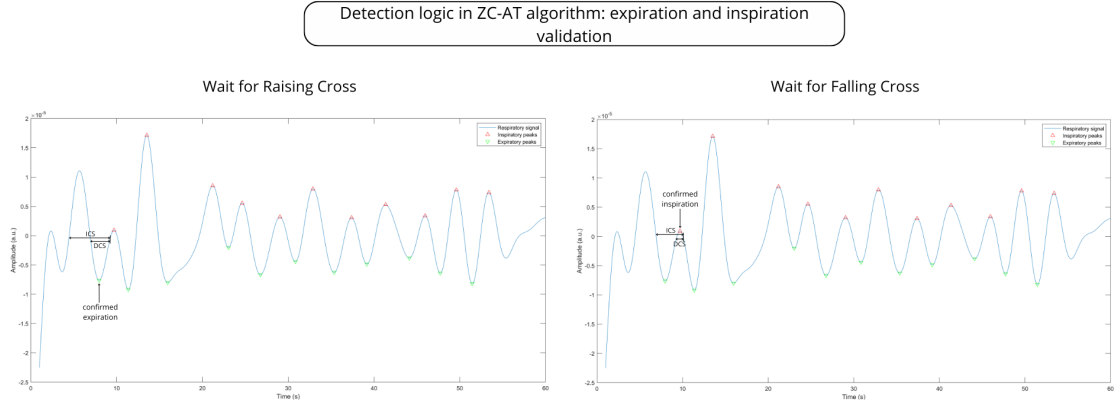


Figure 3.11: Detection logic in the ZC-AT algorithm. The left panel shows the confirmation of an expiratory peak (minimum) while in the WRC state; the right panel shows the confirmation of an inspiratory peak (maximum) in the WFC state. In both cases, ICS and DCS criteria are used to validate the zero-crossing as a true respiratory extremum.

3.5 Estimation of Cardiac Latencies

Cardiac latencies were computed to quantify the temporal relationship between the electrical activation of the ventricles and the corresponding acoustic events associated with cardiac valve closure. For each cardiac cycle, four primary latencies were defined as the time intervals between the R-wave of the ECG and the main components of the heart sounds, corresponding to the mitral (S_{1m}), tricuspid (S_{1t}), aortic (S_{2a}), and pulmonary (S_{2p}) valve closures. These latencies, expressed in milliseconds, represent the electromechanical delays characterizing the onset and progression of the cardiac mechanical response following ventricular depolarization.

3.5.1 Global estimation of cardiac latencies

Cardiac latencies were first estimated over the entire recording without distinction of respiratory phase, in order to obtain a global characterization of the temporal relationship between electrical activation and the corresponding acoustic events. ECG and PCG signals were processed following the same procedure described in Section 3.3.4, which included high-order filtering, R-peak detection, segmentation and artifact rejection of the main heart sound components. For each subject, the latency values were expressed in milliseconds and averaged across all valid beats to compute mean and standard deviation for each component.

This global analysis provided a baseline reference for subsequent comparisons, enabling the assessment of potential respiratory-related modulations in cardiac mechanical timing.

3.5.2 Respiration-conditioned estimation of cardiac latencies

To investigate the influence of respiration on cardiac mechanical timing, the temporal relationship between electrical activation and valvular events was analyzed as a function of the respiratory phase. The respiratory reference signal used for all analyses was derived from the norm of the triaxial accelerometer, as it directly reflects thoracic movements associated with the breathing cycle. This signal was considered the most suitable for identifying the respiratory phase. Specifically, it was used to identify the characteristic points corresponding to the minimum and maximum thoracic expansion, which respectively denote the end of expiration and the end of inspiration. The rationale for excluding the other extracted respiratory signals from the phase-based analysis is presented in the Results and further addressed in the Discussion. To synchronize it with the ECG and PCG signals, originally sampled at 1000 Hz, the respiratory signal (at 25 Hz) was resampled to match this rate. To minimize edge artifacts during resampling, a symmetric reflection padding of 10 samples was applied at both ends and removed after interpolation. This ensured sample-level temporal correspondence between respiratory and cardiac signals, allowing each R-peak to be accurately assigned to the inspiratory or expiratory phase. The R-peak was selected as the temporal anchor because it marks the onset of ventricular depolarization and precedes the mechanical and acoustic events associated with valve closure, providing a physiologically consistent reference point for assessing potential respiration-dependent modulations in electromechanical timing. This enabled the synchronization of cardiac activity with the underlying respiratory dynamics and the subsequent conditioning of cardiac latency estimation on respiratory phase. Building on this framework, three complementary methods were implemented to relate cardiac cycles to respiration, either by classifying beats according to their instantaneous respiratory phase, by linking them to specific respiratory extrema, or by defining phase-dependent intervals within the breathing cycle. The following subsections describe these approaches in detail.

3.5.3 Method A: Phase-based classification of cardiac cycles

In this approach, cardiac latencies were analyzed as a function of the instantaneous respiratory phase, rather than exclusively in relation to the extremes of the respiratory signal. The respiratory signal, obtained from the norm of the triaxial accelerometer, was used to identify the sequence of end-expiration and end-inspiration points, corresponding to the minima and maxima of thoracic expansion, respectively. These reference points defined consecutive respiratory windows, delimited by adjacent pairs of minima and maxima, representing the inspiratory and expiratory phases. Each R-peak detected on the ECG was subsequently associated with the respiratory phase in which it occurred. Beats occurring between a minimum and the subsequent maximum were classified as inspiratory, whereas those between a maximum and the subsequent minimum were classified as expiratory. For R-peaks coinciding exactly with a respiratory extreme, phase attribution followed a physiological logic of continuity: beats at the end of inspiration were still considered part of the inspiratory phase, while those at the end of expiration were assigned to the expiratory phase. This procedure enabled a continuous classification of cardiac cycles in relation to the underlying respiratory dynamics, providing a detailed framework for evaluating potential modulation of electromechanical latencies throughout the entire breathing cycle. An example of this classification is shown in Figure 3.12, where each R-peak is labeled according to its respiratory phase based on the accelerometric reference signal.

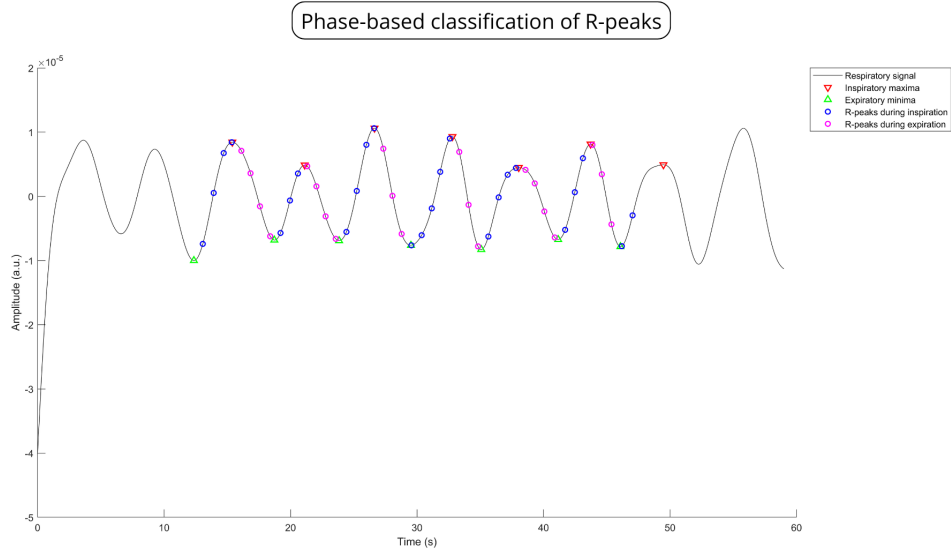


Figure 3.12: R-peak classification based on respiratory phase. Each R-peak was assigned to inspiration or expiration according to its location within respiratory windows delimited by adjacent minima and maxima of the respiratory signal.

3.5.4 Method B: Latency estimation around respiratory maxima and minima

In this approach, cardiac latencies were estimated in proximity to the points of maximum and minimum thoracic expansion, with the aim of analyzing the temporal behavior of electromechanical events near respiratory transitions. For each respiratory extremum identified from the accelerometric reference signal, the closest R-peak in the ECG trace was selected, considering both inspiratory and expiratory phases. To ensure adaptive selection of representative beats, the temporal distance between each respiratory extremum and its nearest R-peak was normalized to the duration of the corresponding respiratory phase. This relative distance metric accounted for individual variability in RR and phase duration across subjects, allowing the comparison of distances in a dimensionless form. For each subject, the threshold was defined as the 90th percentile of the relative distance distribution, ensuring adaptive selection based on individual respiratory dynamics. Beats with relative distances above this level were still part of the same respiratory phase but occurred farther from the corresponding extremum, typically around or beyond the midpoint of the phase, and were therefore considered less representative of the local electromechanical coupling near the respiratory boundary. Special attention was given to edge cases, such as when an R-peak coincided exactly with a respiratory extremum or when the phase duration could not be computed (e.g., at the beginning or end of the recording). In the former case, the distance was set to zero and the beat was automatically retained, as it represented a perfect temporal correspondence between cardiac and respiratory events. In the latter case, the phase duration was undefined, and these beats were excluded to ensure consistent and reliable threshold estimation. This procedure ensured that the estimation of cardiac latencies focused on beats temporally close to the respiratory extrema, either at or immediately adjacent to end-inspiration and end-expiration, thus providing a physiologically consistent assessment of latency modulation across respiratory transitions. An example of this procedure is illustrated in Figure 3.13, where accepted and rejected beats are shown in relation to respiratory extrema.

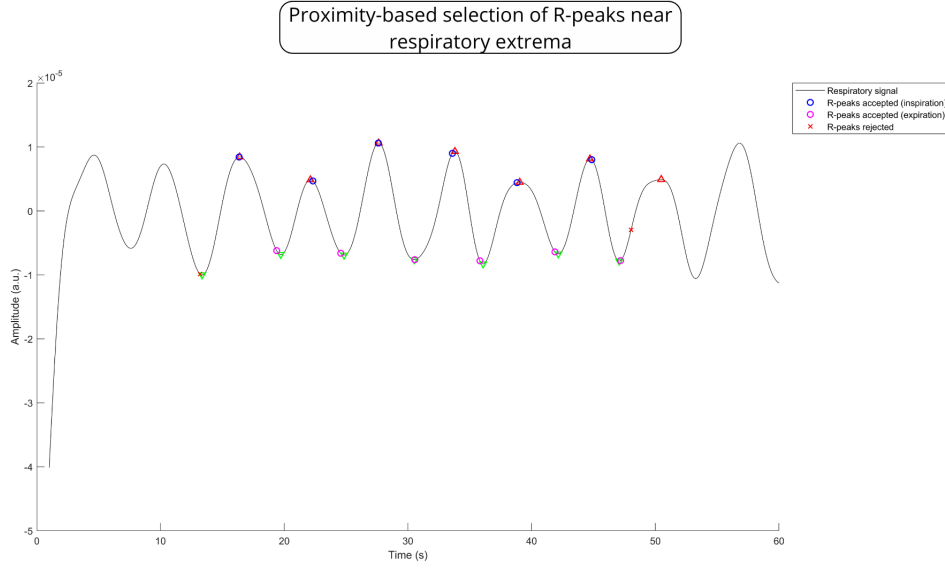


Figure 3.13: Selection of R-peaks near respiratory extrema. For each minimum and maximum of the respiratory signal, the nearest R-peak was identified and retained if its relative distance fell below the threshold computed individually for each subject. Accepted beats are shown as empty circles and color-coded according to their phase, while rejected beats are indicated with red crosses.

3.5.5 Method C: Latency estimation before and after respiratory transitions

This approach aims to directly assess the variation of cardiac latencies at the transitions between inspiration and expiration. Based on the indices of the maxima and minima of the respiratory signal, corresponding respectively to the end of inspiration and the end of expiration, the two cardiac beats closest to each respiratory extremum were identified: the one immediately preceding and the one immediately following. In this way, two representative latency measurements were obtained for each respiratory transition point, one corresponding to the physiological condition preceding the transition (before the extremum) and one following it (after the extremum). The beats were then classified into four distinct configurations: before minimum expansion, after minimum expansion, before maximum expansion, and after maximum expansion. All latency values were expressed in milliseconds and analyzed separately for each respiratory condition to evaluate potential variations in cardiac mechanical timing across consecutive respiratory transitions. This method allows a direct comparison of the electromechanical behavior of the heart in the phases immediately adjacent to changes in the direction of respiratory flow, highlighting possible discontinuities or asymmetries in the modulation of cardiac latencies. Moreover, it provides a useful reference for assessing the stability of latency measures across respiratory cycles and identifying differences in cardiac response during transitions between inspiration and expiration. A visual representation of this classification strategy is provided in Figure 3.14.

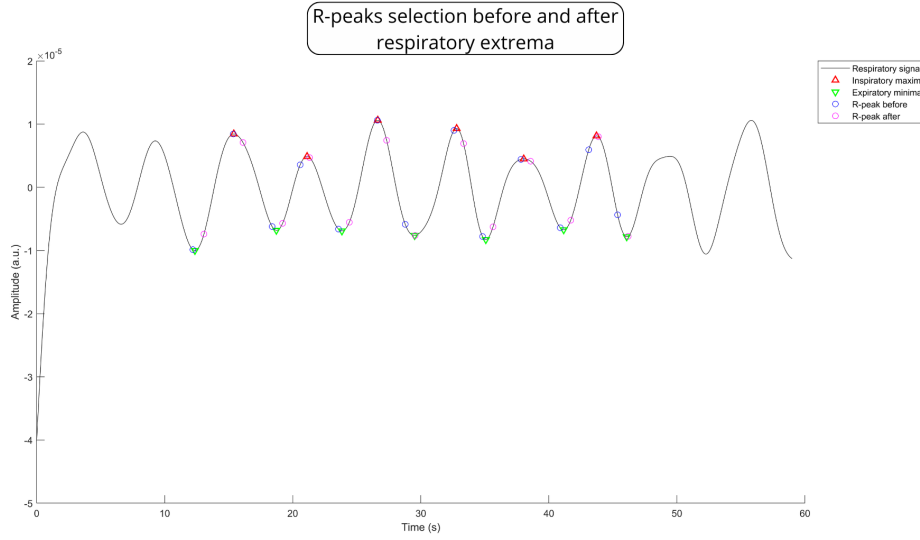


Figure 3.14: R-peaks before and after respiratory extrema. For each maximum or minimum of the respiratory signal, the corresponding R-peaks immediately preceding and following the extremum are shown, together with their assignment to inspiratory or expiratory transitions.

3.5.6 Estimation of Cardiac Time Intervals

CTIs were derived from the previously computed cardiac latencies to quantify the mechanical timing of ventricular function. To enable meaningful comparisons, the CTIs estimated in this study were derived from the same latency definitions reported in [66], where the temporal distances between ECG R-wave and the components of S_1 and S_2 were computed. Specifically, electromechanical activation time (EMAT) was defined as the interval between the R-wave and the onset of the mitral component of S_1 ($R-S_{1m}$), while LVST and the right ventricular ejection time (RVST) corresponded respectively to the durations between S_{1m} and S_{2a} , and between S_{1t} and S_{2p} . The S_1 -split and S_2 -split were computed as the temporal differences between the two components of each heart sound, namely between S_{1t} and S_{1m} , and between S_{2p} and S_{2a} , respectively. For each recording, mean and standard deviation values were calculated over all valid cardiac events, both globally and separately for inspiratory and expiratory phases. Although the analysis in this study focuses on the CTIs, the validation was conducted by comparing the latency values (i.e., $R-S_{1m}$, $R-S_{1t}$, $R-S_{2a}$, $R-S_{2p}$) with those reported in [66], as they represent the fundamental components from which the CTIs are derived. Table 3.3 reports the reference values of these latencies, providing a consistent physiological benchmark for the computed intervals.

Table 3.3: Latency values derived from ECG and PCG signals, as reported in [66]. The 95% confidence intervals are calculated from subject-level means.

| Latency | Mean \pm SD (ms) | 95% Range (ms) |
|------------|--------------------|----------------|
| $R-S_{1m}$ | 43.9 ± 11.4 | 19.5–63.6 |
| $R-S_{1t}$ | 76.0 ± 16.3 | 54.2–115.9 |
| $R-S_{2a}$ | 371.3 ± 21.2 | 333.6–417.0 |
| $R-S_{2p}$ | 399.4 ± 27.6 | 347.4–450.9 |

3.6 Interpretation of CTIs Variations

Since no universally accepted clinical thresholds exist for most CTIs, and because individual physiological variability further complicates the definition of fixed cut-off values, the literature does not offer directly applicable references. As a consequence, no absolute threshold is introduced in this study to assess the relevance of respiratory-induced changes. The confidence intervals reported in [66] describe the inter-subject variability of latency measures obtained with the same device and protocol. In the present work, they are therefore used exclusively to validate the plausibility of the extracted latencies, which represent the fundamental timing components of each CTI. Respiratory effects on CTIs are instead quantified through signed relative variations between phase-specific and global estimates, expressed as percentage changes. Since group-level aggregation may conceal opposing subject-specific behaviours, masking increases in some subjects with decreases in others, the assessment of respiratory modulation is performed at the intra-subject level. This approach ensures that respiratory effects are evaluated according to each individual’s baseline timing, avoiding compensation phenomena that would otherwise flatten the sample-level distributions. For each subject and CTI, the relative variation is defined as:

$$\Delta_{\%} = \frac{CTI_{\text{phase}} - CTI_{\text{global}}}{CTI_{\text{global}}} \times 100 \quad (3.4)$$

This formulation preserves the direction of change, indicating whether the respiratory phase increases or decreases the interval, while providing a scale-independent measure of modulation. Since no intra-subject physiological thresholds exist for CTIs, the interpretation focuses on the consistency and relative magnitude of these variations across subjects and parameters rather than on absolute significance criteria.

Limitations of External Clinical References

Clinical values reported in the literature often derive from heterogeneous measurement modalities (e.g., echocardiography), use distinct temporal references (such as the Q-wave instead of the R-peak), and involve populations with wide age ranges or specific cardiac conditions. These differences affect the definition and magnitude of reported intervals, making such references unsuitable for direct comparison with the present dataset.

Reference Timing: Q-Wave vs R-Wave

The onset of ventricular depolarisation is not uniformly defined across studies. While several works use the beginning of the QRS complex as temporal reference, this study consistently adopts the R-peak, following the protocol established in [66]. Although physiologically the Q-wave marks the true onset of depolarisation, it is frequently small or absent in healthy individuals. The R-peak therefore provides a more robust and reproducible reference for beat-wise analysis, ensuring consistent CTIs estimation even in noisy conditions.

Chapter 4

Results

4.1 Respiratory Rate Estimation Across Methods

The respiratory rate was estimated for each subject and extraction method as the inverse of the average respiratory cycle duration, as described in Section 3.3.6. Tables 4.1 and 4.2 report the respiratory rates values, expressed in bpm, computed across the ten subjects. To complement the numerical values reported in Tables 4.1 and 4.2, Figures 4.1 and 4.2 illustrate the same data using scatter plots. These visualisations provide an immediate overview of the variability across methods and subjects, highlighting the degree of agreement or divergence relative to the accelerometer-based reference method, which extracts the respiratory signal from the norm of the acceleration vector. For clarity of comparison, the methods are indexed as follows: Method 1 refers to the respiratory signal extracted from the norm of the triaxial acceleration, which serves as the reference signal in this study. Methods 2 and 3 are based on ECG-derived features (RR-intervals and AM, respectively). Methods 4 and 5 rely on the timing of PCG heart sounds (S_1 and S_2). Finally, Methods 6 to 9 correspond to the latencies between the R-wave and characteristic cardiac events: mitral component of S_1 (RS_{1m} , Method 6), tricuspid component of S_1 (RS_{1t} , Method 7), aortic component of S_2 (RS_{2a} , Method 8), and pulmonary component of S_2 (RS_{2p} , Method 9).

Table 4.1: Estimated respiratory rate (bpm) for each subject – Methods 1 to 5.

| Subject | Method 1 ACC-norm | Method 2 RR | Method 3 ECG-AM | Method 4 S1S1 | Method 5 S2S2 |
|---------|----------------------|----------------|--------------------|------------------|------------------|
| subj_01 | 15.7 | 10.1 | 15.8 | 11.7 | 10.1 |
| subj_02 | 10.2 | 11.4 | 14.3 | 10.7 | 10.0 |
| subj_03 | 11.6 | 9.4 | 15.4 | 10.9 | 12.0 |
| subj_04 | 12.6 | 12.6 | 13.2 | 12.7 | 12.6 |
| subj_05 | 13.7 | 14.9 | 14.9 | 14.9 | 15.9 |
| subj_06 | 15.6 | 9.3 | 12.0 | 12.3 | 7.8 |
| subj_07 | 15.3 | 10.1 | 17.0 | 9.2 | 8.4 |
| subj_08 | 17.0 | 14.7 | 16.1 | 15.8 | 14.4 |
| subj_09 | 12.4 | 7.2 | 13.2 | 11.9 | 7.3 |
| subj_10 | 10.6 | 10.6 | 10.7 | 10.7 | 10.6 |

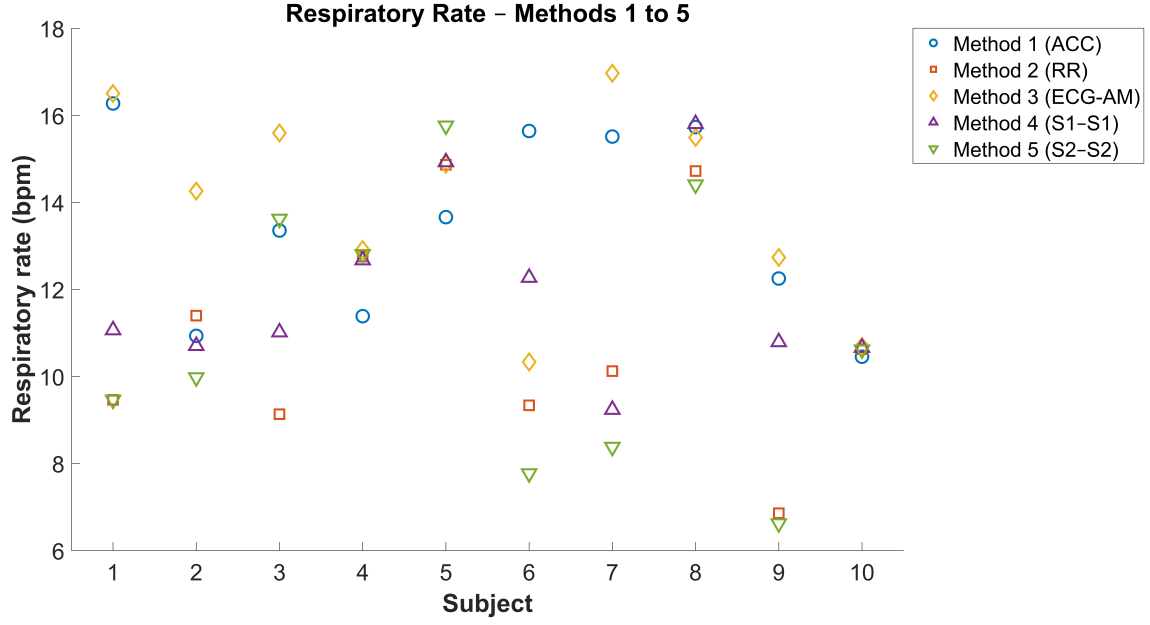


Figure 4.1: Scatter plot of the estimated respiratory rate across subjects for Methods 1 to 5.

Table 4.2: Estimated respiratory rate (bpm) for each subject – Methods 1 and 6 to 9.

| Subject | Method 1 ACC-norm | Method 6 RS _{1m} | Method 7 RS _{1t} | Method 8 RS _{2a} | Method 9 RS _{2p} |
|---------|----------------------|------------------------------|------------------------------|------------------------------|------------------------------|
| subj_01 | 15.7 | 15.9 | 13.5 | 14.7 | 16.5 |
| subj_02 | 10.2 | 11.2 | 10.5 | 15.4 | 11.5 |
| subj_03 | 11.6 | 10.8 | 12.0 | 13.4 | 9.5 |
| subj_04 | 12.6 | 12.9 | 9.6 | 13.5 | 12.0 |
| subj_05 | 13.7 | 13.6 | 13.6 | 13.1 | 13.6 |
| subj_06 | 15.6 | 13.8 | 15.4 | 13.9 | 13.5 |
| subj_07 | 15.3 | 18.6 | 12.9 | 13.6 | 14.1 |
| subj_08 | 17.0 | 9.9 | 11.2 | 10.6 | 12.3 |
| subj_09 | 12.4 | 12.1 | 12.1 | 10.3 | 10.1 |
| subj_10 | 10.6 | 12.3 | 10.6 | 9.9 | 11.2 |

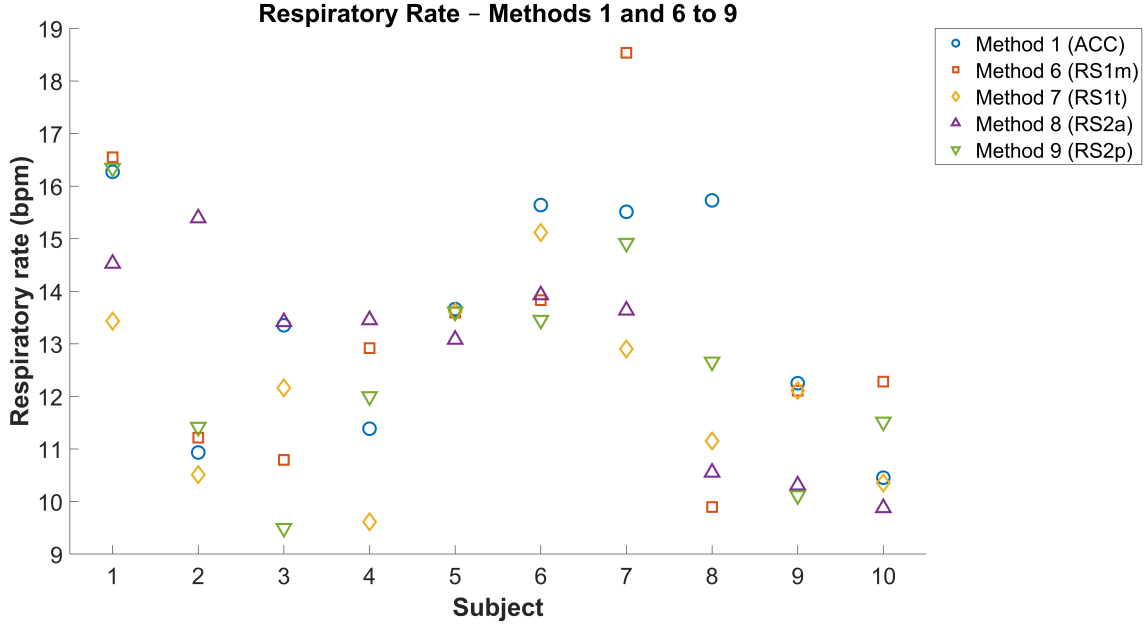


Figure 4.2: Scatter plot of the estimated respiratory rate across subjects for Methods 1 and 6 to 9.

When comparing cardiac-derived estimates with accelerometric reference (Method 1), distinct behaviors emerge between the different modalities. Regarding the ECG and PCG approaches (Table 4.1), the agreement with the reference is highly subject-dependent. In subjects such as subj_04 and subj_10, all methods (1-5) provide remarkably consistent estimates, with variations generally below 1 bpm. However, significant disparities are observed in other cases. For instance, Method 2 (ECG-RR-intervals) and Methods 4-5 (PCG) tend to underestimate the respiratory rate in subjects with higher reference rates (e.g., subj_06 and subj_07), whereas Method 3 (ECG-AM) often yields values closer to or slightly higher than the reference (e.g., subj_01: 15.8 bpm vs. 15.7 bpm; subj_07: 17.0 bpm vs. 15.3 bpm). Focusing on the latency-based methods (Table 4.2), similar variability is evident. In subj_05, the latency estimates (Methods 6-9) are highly consistent with Method 1. Conversely, substantial discrepancies are found in other subjects. A notable example is subj_08, where the reference indicates a rate of 17.0 bpm, while all latency-based methods significantly underestimate this value (ranging from 9.9 to 12.3 bpm). Similarly, isolated variations occur, such as the overestimation by Method 8 in subj_02 (15.4 bpm vs. 10.2 bpm reference). This behaviour is clearly visible in the scatter distribution shown in Fig. 4.1, where the spread between methods varies markedly across subjects: some exhibit tight clustering around the reference value, while others show wider dispersion, particularly for Methods 2, 4, and 5. A similar pattern emerges for the latency-based estimates (Fig. 4.2), with subjects such as subj_05 showing close alignment across methods, whereas others (e.g., subj_08) display a pronounced separation between the reference and the cardiac-derived estimates. Overall, while the cardiac-derived methods often reflect the reference respiratory rate trend, the accuracy of the estimation relative to the accelerometer varies across subjects and extraction techniques.

4.2 Inter-subject Distribution of CTIs

To evaluate the impact of respiratory phase on cardiac time intervals, a series of boxplots was generated for each CTIs. Each plot displays the distribution of subject-level mean

values across the respiratory conditions defined according to the different R-peak selection criteria. These include the global condition, in which cardiac events were considered without associating them to any respiratory phase, and the phase-specific conditions based on the classification of each event as occurring during inspiration or expiration. The number and definition of these conditions vary depending on the approach described in Section 3.5. The total number of valid cardiac events accumulated across the entire subject sample for each condition is indicated above the corresponding box. This visual representation allows assessing the consistency and variability of CTIs values across the different selection strategies.

EMAT

Figure 4.3 displays the distribution of subject-level mean EMAT values across the global and respiration-based conditions for the three methods (A, B, and C). The median EMAT values are consistently aligned across all conditions and methods, ranging approximately between 20 and 25 ms. The inter-subject variability (represented by the interquartile range) appears comparable between the global baseline and the phase-specific subsets. Regarding the respiratory phases, the expiration conditions in Methods B and C exhibit a slightly larger dispersion compared to the inspiration conditions, whereas Method A shows a more balanced distribution between phases. Overall, the central tendency of the EMAT estimates remains stable regardless of the respiratory phase or the calculation method employed.

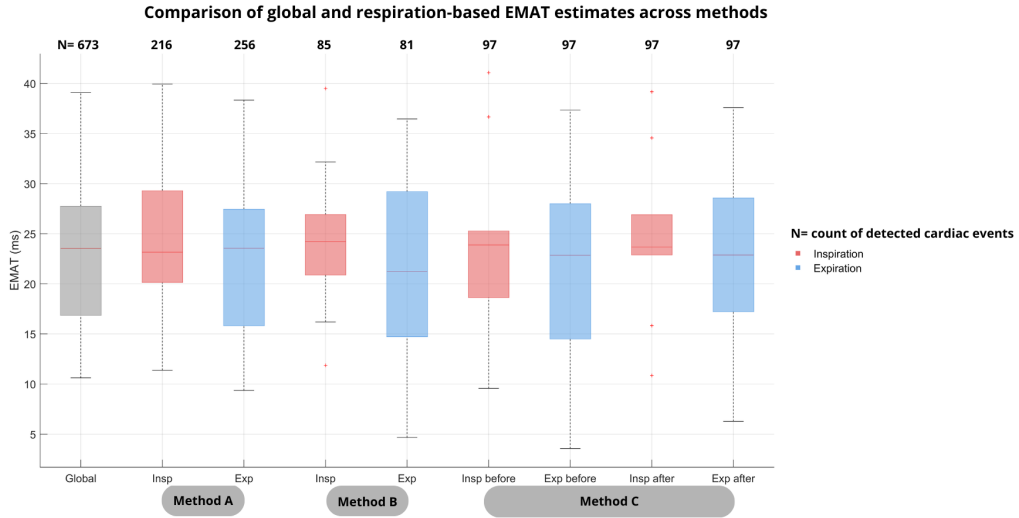


Figure 4.3: Distribution of subject-level mean values of EMAT across respiratory conditions defined according to the selection criteria described in Section 3.5. Each box represents the inter-subject variability for a given condition. The values indicated above the boxes (N) represent the total number of detected cardiac events accumulated across all subjects for each condition.

LVST

Figure 4.4 illustrates the distribution of subject-level mean LVST values across the global and respiration-based conditions. The median values are consistently located in the physiological range of roughly 300-350 ms across all selection methods. The inter-subject variability appears stable across the different conditions. The substantial overlap between the

distributions indicates that the respiratory phase does not induce a distinct or systematic shift in LVST estimates.

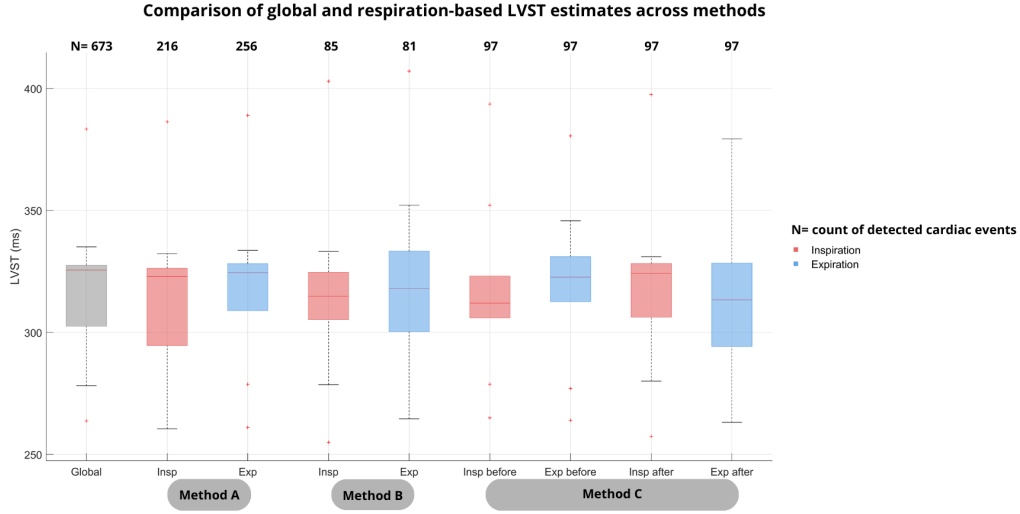


Figure 4.4: Distribution of subject-level mean values of LVST across respiratory conditions defined according to the selection criteria described in Section 3.5. Each box represents the inter-subject variability for a given condition. The values indicated above the boxes (N) represent the total number of detected cardiac events accumulated across all subjects for each condition.

RVST

Figure 4.5 presents the distribution of subject-level mean RVST values across the global and respiratory conditions. The median values generally center around 290-320 ms. Similar to LVST, the RVST estimates show considerable inter-subject variability. When comparing respiratory phases, the behavior appears variable across methods. For instance, in Method C, the relationship between inspiration and expiration inverts between the *before* and *after* conditions (with expiration showing higher median values in the former and lower in the latter). This inconsistent behavior across methods and conditions highlights the absence of a systematic trend distinguishing the respiratory phases in the analyzed data.

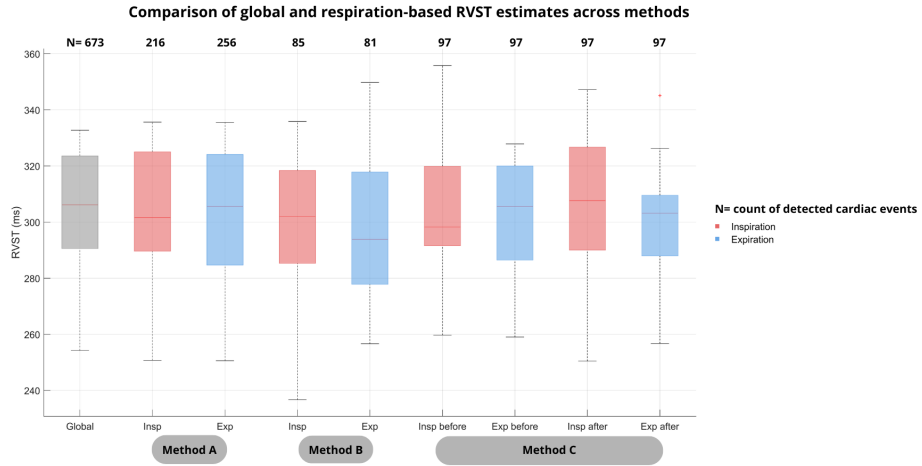


Figure 4.5: Distribution of subject-level mean values of RVST across respiratory conditions defined according to the selection criteria described in Section 3.5. Each box represents the inter-subject variability for a given condition. The values indicated above the boxes (N) represent the total number of detected cardiac events accumulated across all subjects for each condition.

S1 split

Figure 4.6 displays the distribution of subject-level mean S_1 -split values across the respiratory conditions. The median values generally fall within the range of 38-45 ms across all methods. The inter-subject variability appears consistent across the different selection strategies, without major disparities between the respiratory phases. The global condition consistently aligns with the central tendency of the phase-specific distributions, confirming that the overall estimation remains stable regardless of the respiratory partitioning..

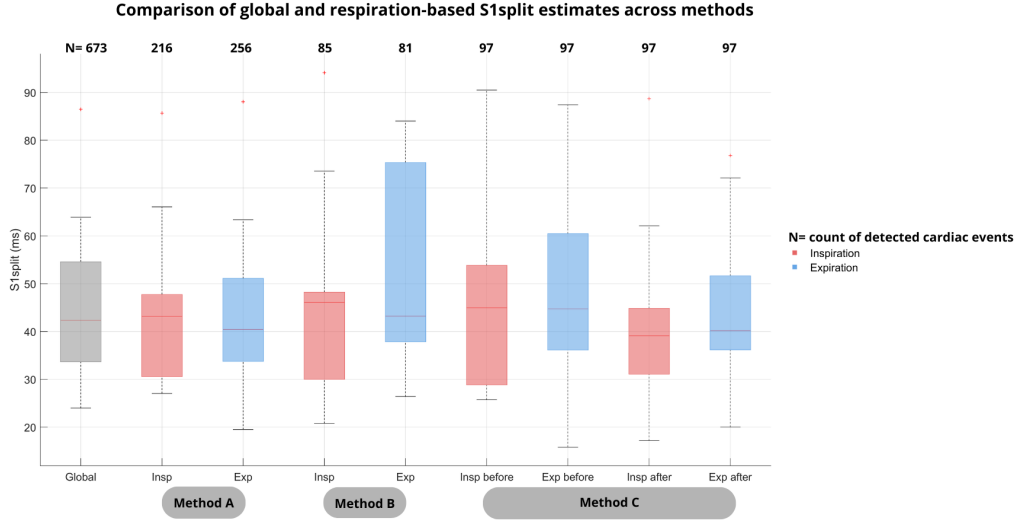


Figure 4.6: Distribution of subject-level mean values of S_1 -split across respiratory conditions defined according to the selection criteria described in Section 3.5. Each box represents the inter-subject variability for a given condition. The values indicated above the boxes (N) represent the total number of detected cardiac events accumulated across all subjects for each condition.

S2 split

Figure 4.7 illustrates the distribution of subject-level mean S_2 -split values across the global and respiratory conditions. The median values are generally positioned between 20-40 ms. The distributions exhibit considerable inter-subject variability. Comparing the respiratory phases, a tendency for higher median values during inspiration compared to expiration is observable in Method A, Method B, and in the *before* condition of Method C. However, this trend is reversed in the *after* condition of Method C, preventing the identification of a universally consistent pattern across all the investigated strategies.

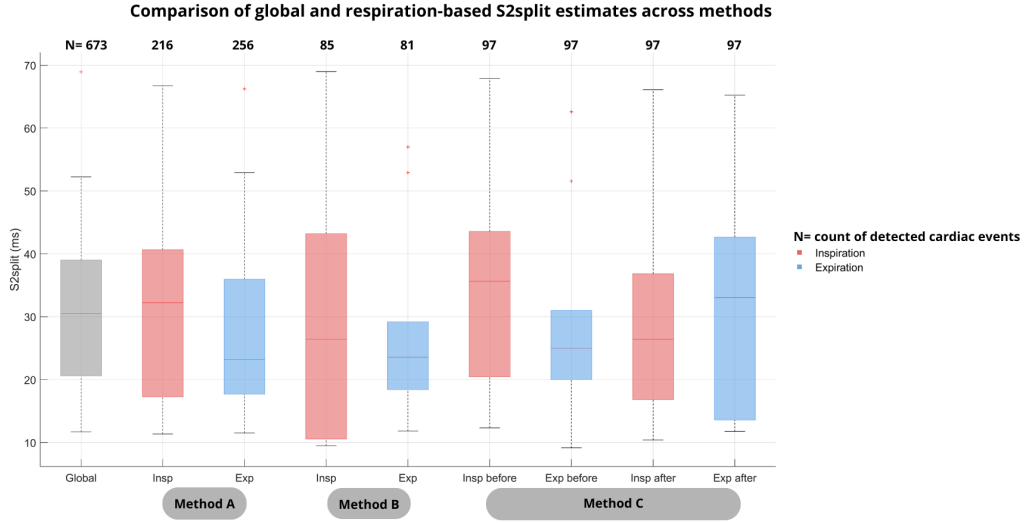


Figure 4.7: Distribution of subject-level mean values of S_2 -split across respiratory conditions defined according to the selection criteria described in Section 3.5. Each box represents the inter-subject variability for a given condition. The values indicated above the boxes (N) represent the total number of detected cardiac events accumulated across all subjects for each condition.

4.3 Global Latency Validation

The table below reports the global mean values of the four reference latencies (RS_{1m} , RS_{1t} , RS_{2a} , RS_{2p}) computed across all subjects, together with the corresponding 95% reference ranges provided in [66]. This comparison allows a direct verification of whether the global measurements obtained in this study fall within the expected physiological intervals. As shown in Table 4.3, all global latency values fall within the corresponding 95% reference ranges reported in [66]. The mean values for all parameters (RS_{1m} , RS_{1t} , RS_{2a} , RS_{2p}) remain entirely contained within the respective intervals, with no cases outside the lower or upper bounds.

Table 4.3: Comparison between the global mean latencies from this study and the 95% reference ranges reported in [66].

| Parameter | Current Study (Global Mean) | Reference (95% Range) |
|-----------|-----------------------------|-----------------------|
| RS_{1m} | 23.5 ms | 19.5 – 63.6 ms |
| RS_{1t} | 69.8 ms | 54.2 – 115.9 ms |
| RS_{2a} | 341.2 ms | 333.6 – 417.0 ms |
| RS_{2p} | 373.9 ms | 347.4 – 450.9 ms |

4.4 Phase-Specific Latency Validation

The table below reports the mean values of the four reference latencies (RS_{1m} , RS_{1t} , RS_{2a} , RS_{2p}) computed separately for inspiration and expiration across all extraction methods (A, B, C-before, C-after). Each phase-specific estimate is shown together with the corresponding 95% reference range reported in [66], allowing a direct comparison between the phase-conditioned measurements and the expected physiological variability. As shown in

Table 4.4, the mean latency values computed separately for inspiration and expiration also remain within the corresponding 95% reference ranges across all parameters and extraction methods.

Table 4.4: Comparison of phase-specific mean latencies (Inspiration vs. Expiration) across extraction methods (A, B, C-before, C-after) with the reference variability ranges.

| Parameter | Method | Inspiration (Mean) | Expiration (Mean) | Reference (95% Range) |
|--------------|------------|--------------------|-------------------|-----------------------|
| RS_{1m} | A | 24.0 ms | 23.3 ms | 19.5 – 63.6 ms |
| | B | 24.6 ms | 20.7 ms | |
| | C (Before) | 24.3 ms | 23.2 ms | |
| | C (After) | 24.7 ms | 23.2 ms | |
| RS_{1t} | A | 69.6 ms | 68.6 ms | 54.2 – 115.9 ms |
| | B | 71.3 ms | 71.5 ms | |
| | C (Before) | 69.3 ms | 67.2 ms | |
| | C (After) | 69.7 ms | 68.3 ms | |
| RS_{2a} | A | 339.7 ms | 341.9 ms | 333.6 – 417.0 ms |
| | B | 341.8 ms | 341.4 ms | |
| | C (Before) | 341.4 ms | 341.3 ms | |
| | C (After) | 342.5 ms | 336.4 ms | |
| 4^*RS_{2p} | A | 373.8 ms | 370.7 ms | 347.4 – 450.9 ms |
| | B | 371.8 ms | 368.7 ms | |
| | C (Before) | 376.5 ms | 372.4 ms | |
| | C (After) | 369.6 ms | 369.9 ms | |

4.5 Subject-Specific Percentage Variations Between Global and Phase-Specific CTIs

To quantify how respiratory phase selection affects the estimation of the CTIs, an intra-subject analysis was performed. For each CTI and for each subject, the signed percentage variation between the phase-specific mean value and the corresponding global mean was computed. This metric reflects both the magnitude and the direction of the variation introduced when restricting the analysis to specific respiratory phases, and it is defined in Eq. 3.4. Methods A and B classify the cardiac cycles into two respiratory conditions (inspiration and expiration), whereas Method C employs the four-condition before/after scheme described in Section 3.5. For every method and for every CTI, the resulting subject-specific variations are reported in the following tables. These values provide a direct quantitative description of how much the CTIs change when estimated within each respiratory condition relative to the global baseline. The observed variations exhibit substantial intra-subject heterogeneity and differ across CTIs and methods, with Method C showing the widest ranges due to its finer phase subdivision. This analysis forms the basis for the interpretation of respiratory modulation effects presented in the Discussion section.

EMAT

Table 4.5: Signed percentage variations of EMAT for Method A during inspiration and expiration.

| Subject | $\Delta_{\%}\text{EMAT}^{\text{insp}} (\%)$ | $\Delta_{\%}\text{EMAT}^{\text{exp}} (\%)$ |
|----------------|---|--|
| subj_01 | 2.4 | -2.0 |
| subj_02 | 17.7 | -4.5 |
| subj_03 | -4.5 | 4.5 |
| subj_04 | 3.8 | -6.6 |
| subj_05 | -5.5 | 5.3 |
| subj_06 | -3.5 | -0.2 |
| subj_07 | 0.3 | 1.5 |
| subj_08 | 11.3 | 0.0 |
| subj_09 | 0.9 | -2.3 |
| subj_10 | 2.3 | -5.8 |

Table 4.6: Signed percentage variations of EMAT for Method B during inspiration and expiration.

| Subject | $\Delta_{\%}\text{EMAT}^{\text{insp}} (\%)$ | $\Delta_{\%}\text{EMAT}^{\text{exp}} (\%)$ |
|----------------|---|--|
| subj_01 | 1.0 | -6.7 |
| subj_02 | 3.9 | 12.8 |
| subj_03 | -0.9 | -10.6 |
| subj_04 | 26.3 | -30.6 |
| subj_05 | 42.8 | -43.0 |
| subj_06 | 0.4 | -5.1 |
| subj_07 | 4.3 | -3.6 |
| subj_08 | 4.5 | -29.7 |
| subj_09 | -19.4 | 12.6 |
| subj_10 | 14.7 | -49.1 |

Table 4.7: Signed percentage variations of EMAT for Method C (Before/After) during inspiration and expiration.

| Subject | $\Delta_{\%}\text{EMAT}^{\text{insp,before}} (\%)$ | $\Delta_{\%}\text{EMAT}^{\text{exp,before}} (\%)$ | $\Delta_{\%}\text{EMAT}^{\text{insp,after}} (\%)$ | $\Delta_{\%}\text{EMAT}^{\text{exp,after}} (\%)$ |
|----------------|--|---|---|--|
| subj_01 | 6.1 | -4.6 | -0.5 | -3.9 |
| subj_02 | 20.7 | -13.9 | -0.1 | 27.6 |
| subj_03 | -15.5 | -6.7 | 14.9 | -11.9 |
| subj_04 | 19.0 | -24.0 | 7.4 | -18.8 |
| subj_05 | 8.7 | -46.3 | 65.7 | -19.4 |
| subj_06 | -3.1 | 1.8 | 0.4 | -8.8 |
| subj_07 | 5.7 | -0.2 | -1.3 | 3.3 |
| subj_08 | 34.6 | -13.3 | -6.8 | 7.8 |
| subj_09 | -22.9 | 0.9 | -3.4 | 30.8 |
| subj_10 | -11.1 | -66.3 | -1.7 | -40.8 |

LVST

Table 4.8: Signed percentage variations of LVST for Method A during inspiration and expiration.

| Subject | $\Delta\%LVST^{\text{insp}}$ (%) | $\Delta\%LVST^{\text{exp}}$ (%) |
|----------------|----------------------------------|---------------------------------|
| subj_01 | -1.0 | 0.3 |
| subj_02 | -0.8 | 1.4 |
| subj_03 | -0.8 | -1.8 |
| subj_04 | -0.9 | 0.1 |
| subj_05 | 0.2 | -0.3 |
| subj_06 | 0.1 | 0.2 |
| subj_07 | 0.6 | -1.3 |
| subj_08 | -1.1 | 0.2 |
| subj_09 | -0.8 | 1.3 |
| subj_10 | -2.0 | 2.4 |

Table 4.9: Signed percentage variations of LVST for Method B during inspiration and expiration.

| Subject | $\Delta\%LVST^{\text{insp}}$ (%) | $\Delta\%LVST^{\text{exp}}$ (%) |
|----------------|----------------------------------|---------------------------------|
| subj_01 | -0.6 | 1.2 |
| subj_02 | 1.7 | -0.1 |
| subj_03 | -3.3 | 0.0 |
| subj_04 | -3.8 | 1.7 |
| subj_05 | 1.5 | -9.6 |
| subj_06 | 0.1 | 1.0 |
| subj_07 | -2.2 | 2.2 |
| subj_08 | -1.6 | 7.6 |
| subj_09 | 5.1 | 6.4 |
| subj_10 | 0.5 | -2.2 |

Table 4.10: Signed percentage variations of LVST for Method C (Before/After) during inspiration and expiration.

| Subject | $\Delta\%LVST^{\text{insp,before}}$ (%) | $\Delta\%LVST^{\text{exp,before}}$ (%) | $\Delta\%LVST^{\text{insp,after}}$ (%) | $\Delta\%LVST^{\text{exp,after}}$ (%) |
|----------------|---|--|--|---------------------------------------|
| subj_01 | -2.0 | 0.7 | 0.0 | 0.5 |
| subj_02 | 0.0 | 1.6 | 2.2 | -1.6 |
| subj_03 | 0.4 | 0.1 | -2.5 | -0.2 |
| subj_04 | -2.0 | 1.1 | -0.6 | 0.3 |
| subj_05 | 7.6 | -3.4 | -1.1 | -9.5 |
| subj_06 | 0.2 | -0.4 | 0.7 | 0.8 |
| subj_07 | -4.0 | -0.8 | -0.7 | 1.1 |
| subj_08 | -4.1 | 5.7 | 0.1 | -1.1 |
| subj_09 | -1.1 | -0.7 | 1.6 | -1.0 |
| subj_10 | 3.6 | 5.8 | 0.2 | -2.7 |

RVST

Table 4.11: Signed percentage variations of RVST for Method A during inspiration and expiration.

| Subject | $\Delta\%RVST^{\text{insp}}$ (%) | $\Delta\%RVST^{\text{exp}}$ (%) |
|----------------|----------------------------------|---------------------------------|
| subj_01 | -0.1 | -0.3 |
| subj_02 | -1.4 | 1.6 |
| subj_03 | -0.8 | -3.0 |
| subj_04 | 0.7 | 0.2 |
| subj_05 | 2.1 | 0.6 |
| subj_06 | -0.6 | -0.9 |
| subj_07 | 1.1 | -3.2 |
| subj_08 | -2.1 | 0.1 |
| subj_09 | 0.7 | -3.9 |
| subj_10 | 0.6 | 1.7 |

Table 4.12: Signed percentage variations of RVST for Method B during inspiration and expiration.

| Subject | $\Delta\%RVST^{\text{insp}}$ (%) | $\Delta\%RVST^{\text{exp}}$ (%) |
|----------------|----------------------------------|---------------------------------|
| subj_01 | -0.4 | 0.7 |
| subj_02 | 2.7 | -5.1 |
| subj_03 | -6.9 | 0.0 |
| subj_04 | -3.0 | -1.8 |
| subj_05 | 3.0 | -16.5 |
| subj_06 | 0.3 | -4.5 |
| subj_07 | -6.0 | -2.9 |
| subj_08 | -2.9 | 5.0 |
| subj_09 | -2.9 | 5.1 |
| subj_10 | 2.9 | -1.8 |

Table 4.13: Signed percentage variations of RVST for Method C (Before/After) during inspiration and expiration.

| Subject | $\Delta\%RVST^{\text{insp,before}}$ (%) | $\Delta\%RVST^{\text{exp,before}}$ (%) | $\Delta\%RVST^{\text{insp,after}}$ (%) | $\Delta\%RVST^{\text{exp,after}}$ (%) |
|----------------|---|--|--|---------------------------------------|
| subj_01 | -0.9 | -0.7 | 0.2 | 0.3 |
| subj_02 | 0.0 | 1.5 | 0.9 | -4.2 |
| subj_03 | 1.5 | 1.9 | -3.1 | 1.0 |
| subj_04 | 0.8 | -1.2 | -0.3 | 0.8 |
| subj_05 | 10.8 | -5.9 | 4.4 | -7.0 |
| subj_06 | -0.3 | -3.3 | 0.3 | -0.8 |
| subj_07 | 0.0 | -1.4 | -2.3 | -0.9 |
| subj_08 | -4.9 | 5.0 | -0.2 | -2.1 |
| subj_09 | -2.5 | -2.4 | -5.2 | 5.3 |
| subj_10 | 5.4 | 1.9 | -0.1 | -0.5 |

S1 split

Table 4.14: Signed percentage variations of S1-split for Method A during inspiration and expiration.

| Subject | $\Delta\%S1\text{-split}^{\text{insp}}$ (%) | $\Delta\%S1\text{-split}^{\text{exp}}$ (%) |
|----------------|---|--|
| subj_01 | -7.0 | 4.1 |
| subj_02 | 29.2 | -19.2 |
| subj_03 | -9.5 | -0.3 |
| subj_04 | -1.8 | -8.2 |
| subj_05 | -12.7 | -5.2 |
| subj_06 | 0.2 | 0.9 |
| subj_07 | -0.3 | 2.9 |
| subj_08 | -11.4 | 0.4 |
| subj_09 | 0.5 | 2.7 |
| subj_10 | 6.5 | -12.3 |

Table 4.15: Signed percentage variations of S1-split for Method B during inspiration and expiration.

| Subject | $\Delta\%S1\text{-split}^{\text{insp}}$ (%) | $\Delta\%S1\text{-split}^{\text{exp}}$ (%) |
|----------------|---|--|
| subj_01 | -3.2 | 4.6 |
| subj_02 | -15.6 | 37.6 |
| subj_03 | -5.0 | -21.1 |
| subj_04 | 9.6 | -3.3 |
| subj_05 | -10.2 | 50.4 |
| subj_06 | -1.1 | 0.9 |
| subj_07 | 11.8 | 17.9 |
| subj_08 | -10.9 | 21.2 |
| subj_09 | 8.9 | -3.6 |
| subj_10 | 3.4 | -3.1 |

Table 4.16: Signed percentage variations of S1-split for Method C (Before/After) during inspiration and expiration.

| Subject | $\Delta\%S1\text{-split}^{\text{insp,before}}$ (%) | $\Delta\%S1\text{-split}^{\text{exp,before}}$ (%) | $\Delta\%S1\text{-split}^{\text{insp,after}}$ (%) | $\Delta\%S1\text{-split}^{\text{exp,after}}$ (%) |
|----------------|--|---|---|--|
| subj_01 | -8.3 | 11.9 | -3.1 | 1.7 |
| subj_02 | 5.6 | -34.0 | -5.5 | 50.8 |
| subj_03 | -7.7 | -17.2 | 8.9 | -33.7 |
| subj_04 | 2.2 | -7.8 | -10.0 | -6.9 |
| subj_05 | -25.2 | 13.9 | -23.2 | -5.4 |
| subj_06 | 1.1 | 5.0 | -3.8 | 1.6 |
| subj_07 | -19.0 | -5.4 | 1.9 | 12.8 |
| subj_08 | -19.5 | 16.4 | -7.4 | -10.9 |
| subj_09 | 13.0 | 1.1 | 8.0 | -11.2 |
| subj_10 | 25.2 | 1.8 | -1.4 | -9.5 |

S2 split

Table 4.17: Signed percentage variations of S2-split for Method A during inspiration and expiration.

| Subject | $\Delta\%S2\text{-split}^{\text{insp}}$ (%) | $\Delta\%S2\text{-split}^{\text{exp}}$ (%) |
|---------|---|--|
| subj_01 | 3.1 | -1.9 |
| subj_02 | 12.0 | -9.6 |
| subj_03 | -14.1 | -14.9 |
| subj_04 | 13.2 | -8.3 |
| subj_05 | -1.6 | 0.6 |
| subj_06 | -3.2 | -3.9 |
| subj_07 | 2.9 | -10.8 |
| subj_08 | -38.0 | -1.3 |
| subj_09 | 18.7 | -49.7 |
| subj_10 | 51.9 | -39.4 |

Table 4.18: Signed percentage variations of S2-split for Method B during inspiration and expiration.

| Subject | $\Delta\%S2\text{-split}^{\text{insp}}$ (%) | $\Delta\%S2\text{-split}^{\text{exp}}$ (%) |
|---------|---|--|
| subj_01 | -3.3 | 1.0 |
| subj_02 | 0.0 | -18.4 |
| subj_03 | -50.0 | -31.3 |
| subj_04 | 18.3 | -36.1 |
| subj_05 | -1.0 | 9.1 |
| subj_06 | 0.1 | -23.2 |
| subj_07 | -9.0 | -13.6 |
| subj_08 | -42.0 | -13.1 |
| subj_09 | -69.3 | -35.3 |
| subj_10 | 40.0 | 2.0 |

Table 4.19: Signed percentage variations of S2-split for Method C (Before/After) during inspiration and expiration.

| Subject | $\Delta\%S2\text{-split}^{\text{insp,before}}$ (%) | $\Delta\%S2\text{-split}^{\text{exp,before}}$ (%) | $\Delta\%S2\text{-split}^{\text{insp,after}}$ (%) | $\Delta\%S2\text{-split}^{\text{exp,after}}$ (%) |
|---------|--|---|---|--|
| subj_01 | 5.5 | -0.2 | -3.0 | 0.5 |
| subj_02 | 3.8 | -20.5 | -13.3 | 9.4 |
| subj_03 | 2.3 | -3.2 | 7.1 | -34.3 |
| subj_04 | 28.8 | -29.8 | -8.9 | -2.9 |
| subj_05 | -5.8 | -1.3 | 11.1 | 11.1 |
| subj_06 | -1.4 | -9.2 | -4.1 | -5.3 |
| subj_07 | 2.4 | -16.0 | -10.0 | 6.3 |
| subj_08 | -45.5 | 13.6 | -18.4 | -35.4 |
| subj_09 | 23.6 | -13.3 | -53.4 | 37.5 |
| subj_10 | 74.8 | -55.6 | -7.8 | 13.1 |

Chapter 5

Discussion

5.1 Reliability of Respiratory Signal Extraction Methods

The extraction of a reliable respiratory signal is a prerequisite for investigating cardiorespiratory coupling. Current literature proposes various methods to derive respiratory rate from cardiac biosignals without the need for additional sensors. In this study, these standard extraction methods were implemented and compared against an accelerometric measurement (Method 1) to evaluate their robustness and consistency. The results obtained from our subject sample reveal a distinct variability in the performance of cardiac-derived methods. Regarding the ECG-based approaches, Method 2 (RR-intervals) showed noticeable underestimations of the respiratory rate in specific healthy subjects (e.g., subj_06 and subj_07). This variability observed in a healthy population points to a broader limitation of the technique: since RR-intervals relies on RSA, its accuracy depends on the magnitude of vagal modulation, which is naturally variable among individuals. From a general clinical perspective, this dependence represents a critical vulnerability. In a broader population including elderly patients or those with cardiac arrhythmias (e.g., atrial fibrillation) and autonomic neuropathy, the physiological coupling required for RSA is severely attenuated or absent [52]. In such cases, the analysis of RR-intervals would fail to carry respiratory information, rendering this method ineffective. Similarly, Amplitude Modulation (Method 3) showed generally better agreement, than the previous described, in our dataset, but it remains subject to morphological limitations reported in the literature. In particular, the amplitude modulation of the QRS complex during respiration is influenced by two main mechanisms: (i) variations in thoracic impedance and (ii) changes in the orientation of the cardiac electrical axis relative to the ECG electrodes [52]. Although these phenomena reflect respiratory activity, they make the technique sensitive to external factors such as posture or signal quality, which can mimic or obscure the respiratory pattern. Furthermore, the presence of irregular ventricular depolarisations (e.g., in arrhythmias) compromises the signal consistency required for this method, limiting its reliability in unselected clinical settings. PCG and latency-based approaches (Methods 4-9) exhibited high inter-subject dispersion in our results. This confirms that isolating respiratory-driven hemodynamic changes from other physiological variability is complex, even in the absence of pathology. In contrast, the respiratory signal extracted from the accelerometer (Method 1) is subject to artifacts primarily related to body movements, which can be managed through filtering. The fundamental advantage of this method lies in its measurement principle: it detects the mechanical expansion of the chest wall. Consequently, unlike cardiac-derived methods, the accelerometer does not depend on the subject's autonomic tone, heart rhythm, or electrical stability.

This independence supports the selection of the accelerometric signal as the reference standard in this study, as it enables consistent respiratory phase detection that is not affected by subject-specific physiological variability.

5.2 Validation of Cardiac Estimates

Before addressing the specific influence of respiration, it is fundamental to assess the baseline plausibility of the extracted cardiac parameters. Since CTIs depend on the differential timing of individual fiducial points, examining these underlying latencies and comparing them with the ranges reported in the reference literature, as described in Section 3.6, allows us to verify that the detected events are physiologically consistent and suitable for further analysis. The latency values obtained in this study for the onset and peak of S_1 and S_2 components were compared with the reference values reported in the validation study by [66]. This comparison is particularly relevant as the reference study utilized the identical wearable device and signal processing methodology.

5.2.1 Global Validation

The consistency of the global mean latencies was assessed by averaging all cardiac events without distinguishing the respiratory phase in which the R-peak occurred. This procedure provided a single average value per subject, from which the overall mean across the ten participants was derived. As shown in Table 4.3 in the Results section, the global mean values obtained in our subject sample consistently fall within the 95% variability range defined by the reference population. The positioning of RS_{1m} towards the lower bound of the reference range is likely attributable to specific population characteristics (e.g., age or body habitus) but remains within the physiological limits of the device.

5.2.2 Phase-Specific Validation

To validate the latency values obtained when cardiac events are associated with a specific respiratory phase, the analysis was repeated separately for inspiration and expiration, based on the methods described in Section 3.5. In particular, for Method C, both the *before* and *after* R-peak selection strategies were evaluated. As demonstrated in Table 4.4 in the Results section, the consistency extends beyond the global average. Across all examined methods, including the distinct processing conditions of Method C, and respiratory phases, the mean latency values remain well within the reference variability ranges. This confirms that the respiratory gating strategy preserves the integrity of the cardiac signal timing. Consequently, the extracted fiducial points are reliable across all conditions, validating the use of these latencies for the subsequent calculation of respiration-dependent CTIs.

5.3 Verification of the Research Hypothesis

The primary objective of this pilot study was to verify the hypothesis that the calculation of CTIs is influenced by the respiratory phase. To address this, we first performed a sample group level descriptive analysis of the distributions, followed by subject-specific analysis.

5.3.1 Group-Level Distribution Analysis

As illustrated in the boxplots presented in Section 4.2 (Figures 4.1-4.5), the distribution of CTIs values appears remarkably stable across all examined conditions. Visually, two main

observations can be drawn:

1. **Respiratory Phase Effects on Closure Timing:** For all parameters (EMAT, LVST, RVST, S_1/S_2 splits), the distributions obtained during inspiration and expiration largely overlap with the global distribution. There is no evident macroscopic shift or separation between the medians of the respiratory phases compared to the global baseline.
2. **Consistency Across Methods:** Despite the methodological differences in respiratory signal extraction and beat classification (Method A, B, and C), the resulting CTIs distributions are consistent. No single method produced systematically divergent estimates, suggesting that the choice of the extraction algorithm does not critically affect the cardiac measurement.

Although these group-level distributions suggest minimal influence of respiration on CTIs, relying solely on pooled data may obscure intra-individual patterns. Opposing trends in different subjects (e.g., an increase in one subject compensating for a decrease in another) could lead to an apparently stable group distribution. To exclude this possibility and rigorously examine the hypothesis, a subject-level quantitative evaluation was conducted to measure, for each individual, how phase-specific estimates differ from the global baseline.

5.4 Subject-Specific Interpretation of Respiratory Modulation on CTIs

The intra-subject percentage variations reported in the tables presented in Section 4.6 show that respiratory phase selection can introduce measurable differences in the CTIs, but these differences do not follow a consistent pattern across subjects or parameters. Most variations remain relatively small, while occasional larger variations appear in isolated cases and in different subjects depending on the CTIs. This irregularity is one of the most characteristic results emerging from the analysis. For EMAT, the majority of subjects display modest percentage changes, with increases and decreases appearing in comparable proportions. Isolated larger values are present, yet they do not recur across subjects or methods, suggesting that they may reflect subject-specific physiological behaviour. LVST shows generally limited variations. Occasional larger shifts appear in a few individuals, but their direction and magnitude differ from case to case, preventing the identification of a shared respiratory pattern. A similar behaviour is observed for RVST, where variations tend to be small in most subjects but can occasionally diverge more noticeably. The presence of positive and negative values within the same parameter suggests that part of this modulation may arise from individual physiological differences rather than from a uniform respiratory mechanism. S_1 split shows a wider spread of percentage variations, especially under Method B and in the before/after subdivision of Method C. However, these larger deviations again do not align across subjects, and both increases and decreases appear in comparable numbers. This lack of consistency makes it difficult to attribute the changes to a reproducible respiratory influence rather than to individual variability or phase-dependent variability of peak detection. S_2 split displays the largest percentage variations, which is coherent with the known physiological modulation of the second heart sound during breathing. Even in this case, however, the direction of the variations differs across individuals, with some showing inspiratory increases and others showing inspiratory decreases. As a result, although respiration clearly interacts with S_2 timing, this interaction does not translate into a uniform trend detectable within this sample. Across all CTIs and methods, the most recurrent element is the absence of a stable, reproducible pattern shared among subjects. Variations are present,

but they appear heterogeneous and subject-specific. Taken together, these observations indicate that within this dataset, respiratory phase does not introduce a consistent shift in CTIs estimation across subjects. Some individuals exhibit noticeable changes, others remain nearly unchanged, and the direction of the variations is not aligned across the sample group.

Chapter 6

Conclusion

6.1 Limitations of the Current Study

The present work is based on a small sample group of healthy subjects, which represents the main limitation of the study. The restricted number of participants prevents any statistical generalisation of the findings, and the observations reported here cannot be interpreted as population-level evidence. The analysis therefore provides descriptive insights rather than statistically supported conclusions.

In addition, the exclusive inclusion of healthy individuals limits the exploration of cardiorespiratory interactions that may emerge more clearly in the presence of altered mechanical or autonomic conditions. As a result, the absence of marked respiratory effects on CTIs in this dataset cannot be extended to different clinical or physiological contexts.

6.1.1 Final Remarks and Future Research Directions

This work should be regarded as a pilot study, in which the full methodological pipeline for the extraction of respiratory phases and CTIs was developed, validated and tested in view of a future expansion to larger datasets. The experimental procedures, the signal processing framework and the comparative analysis across respiratory conditions were established to allow the investigation to be scaled to broader and more heterogeneous populations.

Within the limits imposed by the small sample size, the results obtained do not reveal a clear or systematic relationship between respiratory phase and CTIs. The intra-subject variability observed across parameters and conditions does not indicate a reproducible modulation attributable to respiration in this group of subjects.

Future studies involving larger cohorts and distinct physiological or clinical populations will be required to determine whether the absence of an evident relationship in the present dataset reflects a genuine lack of effect or the limitations associated with the restricted sample examined here.

Bibliography

- [1] Muthiah Vaduganathan, George A. Mensah, Justine Varieur Turco, Valentin Fuster, and Gregory A. Roth. The global burden of cardiovascular diseases and risk. *Journal of the American College of Cardiology*, 80(25):2361–2371, December 2022.
- [2] Junbin Zang, Qi An, Bo Li, Zhidong Zhang, Libo Gao, and Chenyang Xue. A novel wearable device integrating ecg and pcg for cardiac health monitoring. *Microsystems and Nanoengineering*, 11(1), January 2025.
- [3] Anuradha Lala, Craig Beavers, Vanessa Blumer, Laprincess Brewer, Diana De Oliveira-Gomes, Sandra B. Dunbar, Hannah Every, Richard Ferraro, Bonnie Ky, James L. Januzzi, Francoise Marvel, Robert J. Mentz, Erin Michos, Jagat Narula, Khuram Nasir, Pradeep Natarajan, Lori Ann Peterson, Fatima Rodriguez, Michael D. Shapiro, Jenna Skowronski, Randall C. Starling, Pam Taub, Ryan J. Tedford, Quentin Youmans, Shelley Zieroth, and Martha Gulati. The continuum of prevention and heart failure in cardiovascular medicine: A joint scientific statement from the heart failure society of america and the american society for preventive cardiology. *Journal of Cardiac Failure*, August 2025.
- [4] Theresa A McDonagh, Marco Metra, Marianna Adamo, Roy S Gardner, Andreas Baumbach, Michael Böhm, Haran Burri, Javed Butler, Jelena Čelutkienė, Ovidiu Chioncel, John G F Cleland, Andrew J S Coats, Maria G Crespo-Leiro, Dimitrios Farmakis, Martine Gilard, Stephane Heymans, Arno W Hoes, Tiny Jaarsma, Ewa A Jankowska, Mitja Lainscak, Carolyn S P Lam, Alexander R Lyon, John J V McMurray, Alexandre Mebazaa, Richard Mindham, Claudio Muneretto, Massimo Francesco Piepoli, Susanna Price, Giuseppe M C Rosano, Frank Ruschitzka, Anne Kathrine Skibelund, Rudolf A de Boer, P Christian Schulze, Magdy Abdelhamid, Victor Aboyans, Stamatis Adamopoulos, Stefan D Anker, Elena Arbelo, Riccardo Asteggiano, Johann Bauersachs, Antoni Bayes-Genis, Michael A Borger, Werner Budts, Maja Cikes, Kevin Damman, Victoria Delgado, Paul Dendale, Polychronis Dilaveris, Heinz Drexel, Justin Ezekowitz, Volkmar Falk, Laurent Fauchier, Gerasimos Filippatos, Alan Fraser, Norbert Frey, Chris P Gale, Finn Gustafsson, Julie Harris, Bernard Iung, Stefan Janssens, Mariell Jessup, Aleksandra Konradi, Dipak Kotecha, Ekaterini Lambrinou, Patrizio Lancellotti, Ulf Landmesser, Christophe Leclercq, Basil S Lewis, Francisco Leyva, Aleš Linhart, Maja-Lisa Løchen, Lars H Lund, Donna Mancini, Josep Masip, Davor Milicic, Christian Mueller, Holger Nef, Jens-Cosedis Nielsen, Lis Neubeck, Michel Noutsias, Steffen E Petersen, Anna Sonia Petronio, Piotr Ponikowski, Eva Prescott, Amina Rakisheva, Dimitrios J Richter, Evgeny Schlyakhto, Petar Seferovic, Michele Senni, Marta Sitges, Miguel Sousa-Uva, Carlo G Tocchetti, Rhian M Touyz, Carsten Tschoepe, Johannes Waltenberger, Marianna Adamo, Andreas Baumbach, Michael Böhm, Haran Burri, Jelena Čelutkienė, Ovidiu Chioncel, John G F Cleland, Andrew J S Coats, Maria G Crespo-Leiro, Dimitrios Farmakis, Roy S Gardner, Martine Gilard, Stephane Heymans, Arno W Hoes, Tiny Jaarsma, Ewa A Jankowska, Mitja Lainscak, Carolyn S P Lam, Alexander R Lyon, John J V McMurray, Alexandre

- Mebazaa, Richard Mindham, Claudio Muneretto, Massimo Francesco Piepoli, Susanna Price, Giuseppe M C Rosano, Frank Ruschitzka, and Anne Kathrine Skibelund. 2021 esc guidelines for the diagnosis and treatment of acute and chronic heart failure. *European Heart Journal*, 42(36):3599–3726, August 2021.
- [5] Clyde W. Yancy, Mariell Jessup, Biykem Bozkurt, Javed Butler, Donald E. Casey, Mark H. Drazner, Gregg C. Fonarow, Stephen A. Geraci, Tamara Horwich, James L. Januzzi, Maryl R. Johnson, Edward K. Kasper, Wayne C. Levy, Frederick A. Masoudi, Patrick E. McBride, John J.V. McMurray, Judith E. Mitchell, Pamela N. Peterson, Barbara Riegel, Flora Sam, Lynne W. Stevenson, W.H. Wilson Tang, Emily J. Tsai, and Bruce L. Wilkoff. 2013 accf/aha guideline for the management of heart failure. *Journal of the American College of Cardiology*, 62(16):e147–e239, October 2013.
- [6] M. S. Nieminen, D. Brutsaert, K. Dickstein, H. Drexler, F. Follath, V.-P. Harjola, M. Hochadel, M. Komajda, J. Lassus, J. L. Lopez-Sendon, P. Ponikowski, and L. Tavazzi. Euroheart failure survey ii (ehfs ii): a survey on hospitalized acute heart failure patients: description of population. *European Heart Journal*, 27(22):2725–2736, April 2006.
- [7] Òscar Miró, Ana García Sarasola, Carolina Fuenzalida, Sofía Calderón, Javier Jacob, Alfons Aguirre, Da M. Wu, Miguel A. Rizzi, Pierre Malchair, Antonio Haro, Sergio Herrera, Víctor Gil, Francisco J. Martín-Sánchez, Pere Llorens, Pablo Herrero Puente, Héctor Bueno, Alberto Domínguez Rodríguez, Christian E. Müller, Alexandre Mebazaa, Ovidiu Chioncel, and Aitor Alquézar-Arbé. Departments involved during the first episode of acute heart failure and subsequent emergency department revisits and re-hospitalisations: an outlook through the novica cohort. *European Journal of Heart Failure*, 21(10):1231–1244, August 2019.
- [8] Jawad H. Butt, Emil L. Fosbøl, Thomas A. Gerds, Charlotte Andersson, John J.V. McMurray, Mark C. Petrie, Finn Gustafsson, Christian Madelaire, Søren Lund Kristensen, Gunnar H. Gislason, Christian Torp-Pedersen, Lars Køber, and Morten Schou. Readmission and death in patients admitted with new-onset versus worsening of chronic heart failure: insights from a nationwide cohort. *European Journal of Heart Failure*, 22(10):1777–1785, March 2020.
- [9] Patricia Javaloyes, Òscar Miró, Víctor Gil, Francisco Javier Martín-Sánchez, Javier Jacob, Pablo Herrero, Koji Takagi, Aitor Alquézar-Arbé, María Pilar López Díez, Enrique Martín, Carlos Bibiano, Rosa Escoda, Cristina Gil, Marta Fuentes, Guillermo Llopis García, José María Álvarez Pérez, Alba Jerez, Josep Tost, Lluís Llauger, Rodolfo Romero, José Manuel Garrido, Esther Rodríguez-Adrada, Carolina Sánchez, Xavier Rossello, John Parissis, Alexandre Mebazaa, Ovidiu Chioncel, and Pere Llorens. Clinical phenotypes of acute heart failure based on signs and symptoms of perfusion and congestion at emergency department presentation and their relationship with patient management and outcomes. *European Journal of Heart Failure*, 21(11):1353–1365, June 2019.
- [10] Josef Stehlik, Carsten Schmalfuss, Biykem Bozkurt, Jose Nativi-Nicolau, Peter Wohlfahrt, Stephan Wegerich, Kevin Rose, Ranjan Ray, Richard Schofield, Anita Deswal, Jadranka Sekaric, Sebastian Anand, Dylan Richards, Heather Hanson, Matthew Pipke, and Michael Pham. Continuous wearable monitoring analytics predict heart failure hospitalization: The link-hf multicenter study. *Circulation: Heart Failure*, 13(3), March 2020.
- [11] Parastoo Dehkordi, Farzad Khosrow-Khavar, Marco Di Rienzo, Omer T. Inan, Samuel E. Schmidt, Andrew P. Blaber, Kasper Sørensen, Johannes J. Struijk, Vahid Zakeri, Prospero Lombardi, Md. Mobashir H. Shandhi, Mojtaba Borairi, John M. Zanetti,

- and Kouhyar Tavakolian. Comparison of different methods for estimating cardiac timings: A comprehensive multimodal echocardiography investigation. *Frontiers in Physiology*, 10, August 2019.
- [12] H. Boudoulas. Systolic time intervals. *European Heart Journal*, 11(suppl I):93–104, January 1990.
- [13] P. Reant, M. Dijos, E. Donal, A. Mignot, P. Ritter, P. Bordachar, P. Dos Santos, C. Leclercq, R. Roudaut, G. Habib, and S. Lafitte. Systolic time intervals as simple echocardiographic parameters of left ventricular systolic performance: correlation with ejection fraction and longitudinal two-dimensional strain. *European Journal of Echocardiography*, 11(10):834–844, July 2010.
- [14] Oddbjørn Brubakk, Terje R. Pedersen, and Kåre Overskeid. Noninvasive evaluation of the effect of timolol on left ventricular performance after myocardial infarction and the consequence for prognosis. *Journal of the American College of Cardiology*, 9(1):155–160, January 1987.
- [15] Kouhyar Tavakolian, Guy A. Dumont, Geoffrey Houlton, and Andrew P. Blaber. Pre-cordial vibrations provide noninvasive detection of early-stage hemorrhage. *Shock*, 41(2):91–96, February 2014.
- [16] John Kreit. Respiratory-cardiovascular interactions during mechanical ventilation: Physiology and clinical implications, April 2022.
- [17] page 279–308. Elsevier, 2022.
- [18] R. A. Wise, J. L. Robotham, and W. R. Summer. Effects of spontaneous ventilation on the circulation. *Lung*, 159(1):175–186, December 1981.
- [19] Sheldon Magder. Heart-lung interaction in spontaneous breathing subjects: the basics. *Annals of Translational Medicine*, 6(18):348–348, September 2018.
- [20] François Feihl and Alain F. Broccard. Interactions between respiration and systemic hemodynamics. part i: basic concepts. *Intensive Care Medicine*, 35(1):45–54, September 2008.
- [21] Fumihiko Yasuma and Jun-ichiro Hayano. Respiratory sinus arrhythmia. *Chest*, 125(2):683–690, February 2004.
- [22] Maja Elstad, Erin L. O’Callaghan, Alex J. Smith, Alona Ben-Tal, and Rohit Ramchandra. Cardiorespiratory interactions in humans and animals: rhythms for life. *American Journal of Physiology-Heart and Circulatory Physiology*, 315(1):H6–H17, July 2018.
- [23] P. G. Katona and F. Jih. Respiratory sinus arrhythmia: noninvasive measure of parasympathetic cardiac control. *Journal of Applied Physiology*, 39(5):801–805, November 1975.
- [24] Michael Klum, Mike Urban, Timo Tigges, Alexandru-Gabriel Pielmus, Aarne Feldheiser, Theresa Schmitt, and Reinhold Orglmeister. Wearable cardiorespiratory monitoring employing a multimodal digital patch stethoscope: Estimation of ecg, pep, lvet and respiration using a 55 mm single-lead ecg and phonocardiogram. *Sensors*, 20(7):2033, April 2020.
- [25] Aubrey Leatham. Splitting of the first and second heart sounds. *The Lancet*, 264(6839):607–614, September 1954.
- [26] Zhu Yongbo, Xu Lijun, and Issah Abubakari Samori. Mechanical vibration monitoring system for electrocardiogram machine based on hilbert-huang transformations. *The Journal of Engineering*, 2022(11):1104–1113, October 2022.
- [27] Zhixing Gao, Yuqi Wang, Xingchen Xu, Chaohong Zhang, Zhiwei Dai, Haiying Zhang, Jun Zhang, and Hao Yang. A portable cardiac dynamic monitoring system in the framework of electro-mechano-acoustic mapping. *IEEE Transactions on Biomedical Circuits and Systems*, page 1–17, 2024.
- [28] Hong J. Lee, Dong S. Lee, Hyun B. Kwon, Do Y. Kim, and Kwang S. Park. Reconstruction of 12-lead ecg using a single-patch device. *Methods of Information in Medicine*,

- 56(04):319–327, 2017.
- [29] Roberto De Fazio, Ilaria Cascella, Şule Esma Yalçinkaya, Massimo De Vittorio, Luigi Patrono, Ramiro Velazquez, and Paolo Visconti. Synchronous acquisition and processing of electro- and phono-cardiogram signals for accurate systolic times’ measurement in heart disease diagnosis and monitoring. *Sensors*, 25(13):4220, July 2025.
 - [30] A.A. Luisada, C.K. Liu, C. Aravanis, M. Testelli, and J. Morris. On the mechanism of production of the heart sounds. *American Heart Journal*, 55(3):383–399, March 1958.
 - [31] P. M. Shah, M. Mori, D. M. Maccanon, and A. A. Luisada. Hemodynamic correlates of the various components of the first heart sound. *Circulation Research*, 12(4):386–392, April 1963.
 - [32] Tsuguya Sakamoto, Reizo Kusukawa, Donald M. Maccanon, Aldo A. Luisada, and Ivan Harvey. Hemodynamic determinants of the amplitude of the first heart sound. *Circulation Research*, 16(1):45–57, January 1965.
 - [33] T. Sakamoto, R. Kusukawa, D. M. MacCanon, and A. A. Luisada. First heart sound amplitude in experimentally induced alternans. *Chest*, 50(5):470–475, 1966.
 - [34] Hong Tang, Yongwan Park, and Chengjie Ruan. Nonlinear time domain relation between respiratory phase and timing of the first heart sound. *Computational and Mathematical Methods in Medicine*, 2015:1–7, 2015.
 - [35] Hong Tang, Huaming Chen, and Ting Li. Discrimination of aortic and pulmonary components from the second heart sound using respiratory modulation and measurement of respiratory split. *Applied Sciences*, 7(7):690, July 2017.
 - [36] H. Liang, S. Lukkarinen, and I. Hartimo. Heart sound segmentation algorithm based on heart sound envelopogram. In *Computers in Cardiology 1997*, pages 105–108, 1997.
 - [37] Ingeborg H. Hansen, Karsten Hoppe, Anna Gjerde, Joergen K. Kanters, and Helge B. D. Sorensen. Comparing twelve-lead electrocardiography with close-to-heart patch based electrocardiography. In *2015 37th Annual International Conference of the IEEE Engineering in Medicine and Biology Society (EMBC)*, page 330–333. IEEE, August 2015.
 - [38] Sofia M. Monteiro and Hugo Plácido da Silva. A novel approach to simultaneous phonocardiography and electrocardiography during auscultation. *IEEE Access*, 11:78224–78236, 2023.
 - [39] H. S. Cho et al. Development of wireless electronic cardiogram and stethoscope (ecgs) to measure ecg signal and heart sound. *Journal of Biomedical Engineering Research*, 43:124–130, 2022.
 - [40] Paris B. Lovett, Jason M. Buchwald, Kai Stürmann, and Polly Bijur. The vexatious vital: Neither clinical measurements by nurses nor an electronic monitor provides accurate measurements of respiratory rate in triage. *Annals of Emergency Medicine*, 45(1):68–76, January 2005.
 - [41] Ian Smith, John Mackay, Nahla Fahrid, and Don Kruckeck. Respiratory rate measurement: a comparison of methods. *British Journal of Healthcare Assistants*, 5(1):18–23, January 2011.
 - [42] Andrew Bates, Martin J. Ling, Janek Mann, and D.K. Arvind. Respiratory rate and flow waveform estimation from tri-axial accelerometer data. In *2010 International Conference on Body Sensor Networks*, page 144–150. IEEE, June 2010.
 - [43] Sara Lapi, Federico Lavorini, Giovanni Borgioli, Marco Calzolari, Leonardo Masotti, Massimo Pistolesi, and Giovanni A. Fontana. Respiratory rate assessments using a dual-accelerometer device. *Respiratory Physiology and Neurobiology*, 191:60–66, January 2014.
 - [44] Alexander M. Chan, Nima Ferdosi, and Ravi Narasimhan. Ambulatory respiratory rate detection using ecg and a triaxial accelerometer. In *2013 35th Annual International*

- Conference of the IEEE Engineering in Medicine and Biology Society (EMBC)*, page 4058–4061. IEEE, July 2013.
- [45] A. R. Fekr, K. Radecka, and Z. Zilic. Tidal volume variability and respiration rate estimation using a wearable accelerometer sensor. In *Proceedings of the 4th International Conference on Wireless Mobile Communication and Healthcare (MobiHealth 2014)*, pages 1–6, Athens, Greece, November 2014. ICST (Institute for Computer Sciences, Social-Informatics and Telecommunications Engineering).
 - [46] Atena Roshan Fekr, Katarzyna Radecka, and Zeljko Zilic. Design and evaluation of an intelligent remote tidal volume variability monitoring system in e-health applications. *IEEE Journal of Biomedical and Health Informatics*, 19(5):1532–1548, September 2015.
 - [47] Atena Roshan Fekr, Majid Janidarmian, Katarzyna Radecka, and Zeljko Zilic. Respiration disorders classification with informative features for m-health applications. *IEEE Journal of Biomedical and Health Informatics*, 20(3):733–747, May 2016.
 - [48] P. D. Hung, S. Bonnet, R. Gillemaud, E. Castelli, and P. T. N. Yen. Estimation of respiratory waveform using an accelerometer. In *Proceedings of the 5th IEEE International Symposium on Biomedical Imaging (ISBI)*, pages 1493–1496, 2008.
 - [49] Anmin Jin, Bin Yin, G. Morren, H. Duric, and R.M. Aarts. Performance evaluation of a tri-axial accelerometry-based respiration monitoring for ambient assisted living. In *2009 Annual International Conference of the IEEE Engineering in Medicine and Biology Society*, page 5677–5680. IEEE, September 2009.
 - [50] Guan-Zheng Liu, Yan-Wei Guo, Qing-Song Zhu, Bang-Yu Huang, and Lei Wang. Estimation of respiration rate from three-dimensional acceleration data based on body sensor network. *Telemedicine and e-Health*, 17(9):705–711, November 2011.
 - [51] S.P. Preejith, Ahamed Jeelani, Paresh Maniyar, Jayaraj Joseph, and Mohanasankar Sivaprakasam. Accelerometer based system for continuous respiratory rate monitoring. In *2017 IEEE International Symposium on Medical Measurements and Applications (MeMeA)*, page 171–176. IEEE, May 2017.
 - [52] Peter H Charlton, Timothy Bonnici, Lionel Tarassenko, Jordi Alastruey, David A Clifton, Richard Beale, and Peter J Watkinson. Extraction of respiratory signals from the electrocardiogram and photoplethysmogram: technical and physiological determinants. *Physiological Measurement*, 38(5):669–690, April 2017.
 - [53] Hong Tang, Jiao Gao, Chengjie Ruan, Tianshuang Qiu, and Yongwan Park. Modeling of heart sound morphology and analysis of the morphological variations induced by respiration. *Computers in Biology and Medicine*, 43(11):1637–1644, November 2013.
 - [54] Priya S. Nandi, Veronica M. Pigott, and David H. Spodick. Sequential cardiac responses during the respiratory cycle: Patterns of change in systolic intervals. *Chest*, 63(3):380–385, March 1973.
 - [55] Rajkumar Dhar, Seena E. Darwish, Sara A. Darwish, Richard H. Sandler, and Hansen A. Mansy. Effect of respiration and exercise on seismocardiographic signals. *Computers in Biology and Medicine*, 185:109600, February 2025.
 - [56] "Noemi Giordano, Gabriella Balestra, Marco Ghislieri, Marco Knaflitz, and Samanta Rosati". Automatic identification of the best auscultation area for the estimation of the time of closure of heart valves through multi-source phonocardiography. In *2022 Computing in Cardiology Conference (CinC)*, CinC2022. Computing in Cardiology, December 2022.
 - [57] Noemi Giordano, Samanta Rosati, Daniele Fortunato, Marco Knaflitz, and Gabriella Balestra. *Personalized Detection of Motion Artifacts for Telemonitoring Applications*. IOS Press, May 2024.
 - [58] Noemi Giordano, Samanta Rosati, Gabriella Balestra, and Marco Knaflitz. A wearable multi-sensor array enables the recording of heart sounds in homecare. *Sensors*, 23(13):6241, July 2023.

- [59] Yue-Der Lin and Ya-Fen Jhou. Estimation of heart rate and respiratory rate from the seismocardiogram under resting state. *Biomedical Signal Processing and Control*, 57:101779, March 2020.
- [60] Stephen Hughes, Haipeng Liu, and Dingchang Zheng. Influences of sensor placement site and subject posture on measurement of respiratory frequency using triaxial accelerometers. *Frontiers in Physiology*, 11, July 2020.
- [61] Sankirna D. Joge. Qrs detection using pan–tompkins algorithm from ecg signal, 2021. Retrieved April 22, 2025.
- [62] Jiapu Pan and Willis J. Tompkins. A real-time qrs detection algorithm. *IEEE Transactions on Biomedical Engineering*, BME-32(3):230–236, March 1985.
- [63] Donghwan Yun, Hyung-Chul Lee, Chul-Woo Jung, Soonil Kwon, So-Ryoung Lee, Kwangsoo Kim, Yon Su Kim, and Seung Seok Han. Robust r-peak detection in an electrocardiogram with stationary wavelet transformation and separable convolution. *Scientific Reports*, 12(1), November 2022.
- [64] C.L. Mason and L. Tarassenko. Quantitative assessment of respiratory derivation algorithms. In *2001 Conference Proceedings of the 23rd Annual International Conference of the IEEE Engineering in Medicine and Biology Society*, IEMBS-01, page 1998–2001. IEEE.
- [65] V. Nivitha Varghees and K.I. Ramachandran. A novel heart sound activity detection framework for automated heart sound analysis. *Biomedical Signal Processing and Control*, 13:174–188, September 2014.
- [66] Noemi Giordano and Marco Knaflitz. A novel method for measuring the timing of heart sound components through digital phonocardiography. *Sensors*, 19(8):1868, April 2019.
- [67] Jiapu Pan and Willis J. Tompkins. A real-time qrs detection algorithm. *IEEE Transactions on Biomedical Engineering*, BME-32(3):230–236, 1985.
- [68] D Khodadad, S Nordebo, B Müller, A Waldmann, R Yerworth, T Becher, I Frerichs, L Sophocleous, A van Kaam, M Miedema, N Seifnaraghi, and R Bayford. Optimized breath detection algorithm in electrical impedance tomography. *Physiological Measurement*, 39(9):094001, September 2018.
- [69] Marc A. Russo, Danielle M. Santarelli, and Dean O’Rourke. The physiological effects of slow breathing in the healthy human. *Breathe*, 13(4):298–309, November 2017.
- [70] Aravind Natarajan, Hao-Wei Su, Conor Heneghan, Leanna Blunt, Corey O’Connor, and Logan Niehaus. Measurement of respiratory rate using wearable devices and applications to covid-19 detection. *npj Digital Medicine*, 4(1), September 2021.